



Effect of Barrier Height on the Design of Stepped Spillway Using Smoothed Particle Hydrodynamics and Particle Image Velocimetry

Aqil Azman^{1a}, Fei Chong Ng^{1b}, Mohd. Hafiz Zawawi^c, Aizat Abas^{1a}, Mohd. Remy Rozainy M. A. Z.^{1d}, Ismail Abustan^d, Mohd. Nordin Adlan^d, and Wei Loon Tam^a

^aSchool of Mechanical Engineering, Universiti Sains Malaysia, Nibong Tebal 14300, Malaysia

^bInstitute of Energy Infrastructure (IEI), Universiti Tenaga Nasional, Kajang 43000, Malaysia

^cDept. of Civil Engineering, Universiti Tenaga Nasional, Kajang 43000, Malaysia

^dSchool of Civil Engineering, Universiti Sains Malaysia, Nibong Tebal 14300, Malaysia

ARTICLE HISTORY

Received 10 August 2018
Revised 16 February 2019
Accepted 24 November 2019
Published Online 10 January 2020

KEYWORDS

SPH
Stepped spillway
PIV
Aeration
Barrier height
Oxygenation performances

ABSTRACT

Three-dimensional stepped spillway problems are simulated numerically using smoothed particle hydrodynamics (SPH) to visualize the flow of water along the steps and its flow dynamics. In particular, two distinct scaled-down stepped spillway models were studied with each having barrier heights of 10 mm and 25 mm, respectively. The impact of varying the height of the barrier in the design of the stepped spillway is studied in terms of its flow pattern, flow dynamics, aeration efficiency and oxygenation performances. State-of-the-art particle image velocimetry (PIV) experiment was carried out to affirm the validity of SPH findings and it turns out that both the water flow patterns attained in the SPH and PIV are quantitatively comparable. Further quantitative analysis revealed that the flow velocities in both methodologies are in great consensus. Conclusively, this has demonstrated that the capability and reliability of SPH to precisely approximate the water using finite set of particles to model the flow along the stepped spillway. Both stepped spillway configurations show nappe flow regime as the water descends down the steps. Nonetheless, vigorous hydraulic jump phenomena that is associated with the formation of turbulence and vortices is prominently observed in the configuration with larger barrier height. Decisive SPH data obtained concluded that as the barrier height increases from 10 mm to 25 mm, the water flows down the steps faster at lower pressure value and the overall aeration efficiency is improved from 1.1% to 1.2%. The usage of the higher barrier would promote the occurrence of substantial air entrainment during water swirling that will increase the power dissipation in flow. Subsequently, this while lower the power drawn to achieve the desired aeration effect. Ultimately, this study has justified the critical influence of barrier height dimension on the stepped spillway flow behavior and aeration performance.

1. Introduction

Stepped spillway is a type of hydrological spillway with steps built on its chute to assist in the dissipation of the kinetic energy of the descending water, through the formation of hydraulic jump (Lawler, 1993). This eliminates the need for additional installment of energy dissipater at the end of the spillway downstream. Moreover, stepped spillway is an integrated part in dam to remove surplus water to prevent overflow (Shahheydari

et al., 2015). Each horizontal step is integrated with an isolated stilling basin at the edge of the hydraulic jump and this kind of cascade structure is also known as pooled stepped chute (Chatila and Jurdi, 2004; Thakare and Tatewar, 2009). Water is then sequentially flown from level to level to allow the dissipation of hydraulic energy efficiently with the presence of hydraulic jump (Kumcu, 2017). Additionally, the stepped transitions do provide a good aeration of water as a result of sufficient amount of air-water mixing (Aras and Berkun, 2010).

CORRESPONDENCE Aizat Abas ✉ aizatabas@usm.my ☒ School of Mechanical Engineering, Universiti Sains Malaysia, Nibong Tebal 14300, Malaysia

© 2020 Korean Society of Civil Engineers

The research methodologies adopted in this paper are aimed to study the stepped spillway cascade aerator system based on three-dimensional smoothed particle hydrodynamics (SPH) code and particle image velocimetry (PIV). SPH is a mesh-free, Lagrangian, pseudo-particle interpolation numerical method that utilizes smoothed estimation of particle properties according to weighted average over neighboring particles in the field of fluid dynamics (Gingold and Monaghan, 1977; Monaghan, 1989). Its particle-based nature is meshless in nature and allows for inter-particle forces to be considered thereby higher accuracy and visualization can be expected. Meanwhile, PIV is a non-intrusive method to identify instantaneous vector field in a cross-sectional fluid flow in a physical flow system. The velocity field can be determined based on the movement of illuminated tracer particles that is being introduced to the flow. PIV translates the continuum Eulerian flow into particle Lagrangian approach to visualize the flow dynamics especially its velocity vector.

SPH numerical studies on stepped spillway has been conducted in the past few years. The pressure distribution on steps located in the non-aerated flow region of a stepped spillway for various discharges of skimming flow situations were investigated using two dimensional SPHysics codes. SPH data which is in-line with the experimental findings obtained are promising and thus demonstrated the capability of SPH methods in simulating free surface flow over hydraulic structures (Husain et al., 2014). SPH method is again applied in the study of a two-dimensional flow field characteristics in open channels stepped spillway using open boundary condition. The SPH simulation is found to be able to predict the free surface flow position and velocity distribution along the chute slope (Husain, 2016). Similarly, SPH simulation has been used on the real dynamic behavior of the free surfaces of water flow in spillways. In particular, two-dimensional SPHERIC Benchmark test case of dam break evolution over wet bed was adopted (Jonsson et al., 2015). Toosi et al. (2015) used two dimensional SPH in their research which is the influence of time scale in free surface flow simulation (Toosi et al., 2015). Two-dimensional free surface flow over a sharp-crested weir is successfully simulated using SPH method and the computed results are validated using experimental reference data. These data show good qualitative agreement that suggest an unsteady evolution of the complex moving material interface produced by the flow field can be visualized using this approach (Ferrari, 2010). Another example of two-dimensional (2D) SPH simulation is conducted on the spillway study of Alarcon Dam, Spain. The flow rate curve along the spillway and pressure variations over the upper spillway face are plotted (Rebollo et al., 2010). Nonetheless, it is noteworthy to emphasize that these SPH studies on stepped spillway are based on the simplified 2D flow domain only due to highly expensive computational cost for three-dimensional (3D) simulation.

Later, there is an attempt to implement the SPH numerical approach to construct the three-dimensional model of weir flow through a four gated, spillway system. This paper demonstrated that SPH is capable of simulating a complex 3D flow in stepped

spillway and to solve complex free surface behavior near the gated structures. Since the SPH simulation models has been compared to experimental setup for validation purpose, it is found that the deviation can be minimized by increasing the partial resolution in SPH study but at a cost of an increase in computational time (Saunders et al., 2014).

Various types of numerical simulation studies have been concerted to study the water flow in stepped spillway. The stepped spillway problem had been simulated based on the Reynolds stress turbulence model to investigate the skimming flow over the steps as well as its pressure and velocity distributions (Chen et al., 2002). Additionally, finite element computational fluid dynamics module, ADINA-F has also been practiced predicting the skimming flow over corner vortices in a stepped spillway of different setup configurations to predict determine its energy dissipation (Tabbara et al., 2005). Apart from that, the stepped spillway model was also simulated using V-Flow simulation in MATLAB to determine the flow streamlines and pressures at various points on the spillway (Vosoughifar et al., 2013). Moreover, the flow velocity and its turbulence intensity in stepped spillway is being investigated based on the two-dimensional Navier-Stokes equations numerically with refined volume-of-fluid (VOF) algorithm and Fractional Area-Volume Obstacle Representation (FAVOR) method (Carvalho et al., 2009). All the findings in these numerical approaches have been validated with corresponding experimental techniques and showed great consensus between both simulation and experimental methodology.

However, the aforementioned elemental numerical methods, of either based on Finite Element or Finite Volume, usually neglect the particles interaction forces, which is one of the crucial aspects of flow simulation. Therefore, the computational results of highest precision possible may not able to be achieved. On contrary, the mesh-less particle method simulation like SPH is expected to have higher resolution and thus better visualization since it eases the movement between particles. This enable the particle-based simulation model to compute for much more accurate values of pressure and velocity.

The use of SPH numerical simulation is not just limited to the stepped spillway. It is reported that the application of SPH is successful in the modelling of dam break flow (Chang et al., 2011; Xu, 2016), flood (Kao and Chang, 2012; Albano et al., 2016), bubble coalescing (Zhang et al., 2015) and non-Newtonian free surface flows (Xu et al., 2013). With all the flows in aforementioned cases able to be precisely simulated, these have proven the versatility of fluid modeling using SPH method.

While there are various experiments being conducted to study the water flow and its characteristic along the stepped spillways, there is one particular state-of-art experimental methodology termed as PIV that is able to provide accurate insight on the velocity vector and its magnitude as well as the streamlines. PIV technique have been applied in various stepped spillway models and applications. For instance, to characterize the flow field in the non-aerated region of the skimming flow regime (Amador et al., 2004), to attain pressure and velocity measurements of flow

(Peltier et al., 2017), as well as to investigate air-water interfacial flow properties, turbulence intensity and energy dissipation in aeration system (Felder and Chanson, 2013). Generally, all validation experiments in the listed literatures previously are rely on scaled-down model of stepped spillway, observing the flow pattern and measures the flow's pressure and velocity using gauge apparatus. It is regarding that PIV is somewhat more sophisticated technique in determine the flow's velocity using imaging system.

On the other hand, the stepped chute configurations and the design of stepped spillway is also being researched extensively an attempt to relate to its cavitation and aeration performances. In-line, staggered, flat and pooled stepped spillway configurations were tested on their cavity flow process, flow aeration and energy dissipation performances (Guenther et al., 2013). It is revealed that lower interfacial velocity and higher energy dissipation are being observed at the flat stepped chute. This study suggested that the flat step design is the most beneficial in terms of the flow stability and energy dissipation performance (Stefan and Hubert, 2014).

Furthermore, the formation air entrainment in stepped chutes is studied to determine the non-aerated flow region which is potentially prone to cavitation damage and the pressure field acting on the step faces. It is found that the negative gauge pressure region is more likely to cause cavitation (António et al., 2009). A study on nappe flow type in the stepped chutes showed that it occurs at low discharge rate and the power dissipation along stepped chutes with the nappe flow regime increases with decreasing discharges (Chanson, 1994). Subsequently, the flow properties in the stepped chutes of various configurations are rigorously studied, aimed to enhance its energy dissipation and minimize the cavitation (Gonzalez and Chanson, 2007; Felder and Chanson, 2011).

Substantial number of researches have also been concerted particularly on the aeration effect and hydraulic jump phenomena in stepped spillway. Theoretically, the aeration effect that is based on the hydraulic jump phenomena is studied and the aeration efficiency is shown to be proportional to the power dissipated in the flow (Kucukali and Cokgor, 2009). Experiments that have been carried out found that the increase in turbulence intensity in air-water flow is proportional to the number of the entrained bubbles observed (Chanson and Toombes, 2002). Another research justified that the optimization on design of aerator via hydraulic modeling is able to reduce the cavitation damage significantly and enhance the air concentration of the bottom flow on the stepped chute (Wang et al., 2012). Moreover, experimental study on the energy dissipation in the stepped spillway of different slopes and dimensions has also been conducted. It is discovered that varying dimensions and design of the stepped spillway will affects its flow regime and eventually it is concluded that the energy dissipated in nappe flow is considerable higher than that in the skimming flow (Hamedi et al., 2012; Roushangar et al., 2014). Further study revealed that for similar flow rate, the energy dissipation increases in model of steeper slope (Mostefa et al., 2015). To

enrich the understanding on this particular subject, plate boundary layer theory is proposed to predict the possible locations of the inception point of air entrainment in the stepped spillway (Wu et al., 2013). Apart from that, the aeration performance of the cascade system for water with and without deoxygenation is also being studied. The study confirmed that the aeration performance will decrease after the flow rate through cascade exceeded the threshold value (Rathinakumar et al., 2014). Subsequently, it is also reported that the increase in the number of steps in stepped spillway will improve the effectiveness of water treatment in aeration (Kokila and Divya, 2015).

Based on the literatures presented so far, the SPH numerical studies on the flow in stepped spillway are rather limited to just two-dimensional model. Furthermore, the study related to the effect of varying the height of the at the edge of spillway chute on flow behavior is found to be limited. Moreover, extensive literature review on relevant subject revealed that the PIV experiment has been scarcely conducted to visualize the flow in stepped spillway. To the best knowledge of the authors, by far there is no study has been conducted to investigate aeration performance and flow dynamics on the stepped spillway of varying the barrier's height that is based on the combination of SPH simulation and PIV experimental flow visualization. These two particle-based approaches are required to conduct side-by-side to accurately predict the flow along the stepped spillway. This is due to the SPH simulation or PIV experiment standalone may insufficient to fully explain the underlying phenomena, in a thoroughly yet accurate manner.

2. Material and Methods

2.1 SPH Numerical Model of Stepped Spillway

2.1.1 Model Configurations

2.1.1.1 SPH Formulations

As a review, SPH involves the computation of discretized fluid into a set of particles, each particle is referred to a nodal point where physical quantity are computed as an interpolation of the values of the nearest particles. The integral approximation of any function $A(\vec{r})$ is:

$$A(\vec{r}) = \int A(\vec{r}') W(\vec{r} - \vec{r}', h) d\vec{r}' \quad (1)$$

In which, h is the smoothing length and $W(r-r', h)$ is the weighting function or smoothing kernel. The function $A(\vec{r})$ can be expressed in the discretized form and the approximation of the function at particle a is given by:

$$A(\vec{r}) = \sum_b m_b \frac{A_b}{\rho_b} W_{ab} \quad (2)$$

In which, m_b and ρ_b being the mass and density associated to the neighboring particle b , respectively. Besides, the term $W_{ab} = W(\vec{r}_a - \vec{r}_b, h)$ describes the weight function.

2.1.1.2 Weighting Function or Smoothing Kernel

The smoothing kernel functions must fulfil several properties such as normalization, compact support and monotonically decreasing with distance from point a when smoothing length, h approaches zero. Various kind of kernel definitions are available and for this particular research, the cubic spline kernel is selected and shown as follow:

$$W(r, h) = \alpha_D \begin{cases} 1 - \frac{3}{2}q^2 + \frac{3}{4}q^3 & 0 \leq q \leq 1 \\ \frac{1}{4}(2-q)^3 & 1 \leq q \leq 2 \\ 0 & q \geq 2 \end{cases} \quad (3)$$

where $\alpha_D = 1/(\pi h^3)$ in three-dimensional flow domain.

2.1.1.3 Momentum Equation

The momentum conservation equation in a continuum Eulerian field is shown as follows:

$$\frac{D\vec{v}}{Dt} = -\frac{1}{\rho}\vec{\nabla}P + \vec{g} + \vec{\Theta} \quad (4)$$

where $\vec{\Theta}$ denotes the diffusion term.

The momentum equation in SPH method can be described by different approaches based on various existing formulations of the diffusive terms. The momentum equation (Monaghan, 1992) is implemented to determine the acceleration of a particle a as a result of the particle interaction with its neighbors, particles b :

$$\frac{d\vec{v}_a}{dt} = -\sum_b m_b \left(\frac{P_b}{\rho_b^2} + \frac{P_a}{\rho_a^2} + \Pi_{ab} \right) \nabla_a W_{ab} + \vec{g} \quad (5)$$

such that v being the velocity, P is the pressure, ρ is the density, m is the mass of particle, $\vec{g} = (0, 0, -9.81) \text{ m/s}^2$ is the three-dimensional gravitational acceleration vector and W_{ab} denotes the kernel function that dependent on the distance between particles a and b .

Generally, in SPH notation, the pressure gradient term in symmetrical form is expressed as:

$$\left(-\frac{1}{\rho} \nabla P \right)_a = -\sum_b m_b \left(\frac{P_b}{\rho_b^2} + \frac{P_a}{\rho_a^2} + \Pi_{ab} \right) \nabla_a W_{ab} \quad (6)$$

where Π_{ab} is the viscosity term which defined as:

$$\Pi_{ab} = \begin{cases} \frac{-\alpha \bar{c}_{ab} \mu_{ab}}{\bar{\rho}_{ab}} & \vec{v}_{ab} \cdot \vec{r}_{ab} < 0 \\ 0 & \vec{v}_{ab} \cdot \vec{r}_{ab} > 0 \end{cases} \quad (7)$$

with $\mu_{ab} = \frac{h \vec{v}_{ab} \cdot \vec{r}_{ab}}{\vec{r}_{ab}^2 + \eta^2}$, where, $\vec{r}_{ab} = \vec{r}_a - \vec{r}_b$, $\vec{v}_a - \vec{v}_b$ being \vec{r}_a and \vec{v}_a the position and velocity corresponding to particle a , $\bar{c}_{ab} = 0.5(c_a + c_b)$ is the average speed of sound, $\bar{\rho}_{ab} = 0.5(\rho_a + \rho_b)$ is the mean density and $\eta^2 = 0.01h^2$. Additionally the α is free parameter that can be changed depending on the problem posed.

2.1.1.4 Continuity Equation

The mass of each particle is set to be constant, so that changes in

fluid density are computed by solving the conservation of mass or continuity in SPH which is given as:

$$\frac{d\rho_a}{dt} = \sum_b m_b \vec{v}_{ab} \cdot \nabla_a W_{ab} \quad (8)$$

2.1.1.5 Equation of State

In the classical SPH formulation, the fluid is treated to be weakly compressible. This allows the use of an equation of state to compute fluid pressure, that is much faster than to solved compared to the conventional Poisson's equation. Pressure is calculated starting from density using Tait's equation of state as shown below:

$$P = B \left[\left(\frac{\rho}{\rho_0} \right)^\gamma - 1 \right] \quad (9)$$

where the constants $B = c_0^2 \rho_0 / \gamma$ and $\gamma = 7$, for such that the reference density, $\rho_0 = 1,000 \text{ kg/m}^3$ and the corresponding speed of sound at this particular reference density, $c_0 = c(\rho = \rho_0) = \sqrt{(\partial P / \partial \rho)|_{\rho_0}}$.

2.1.1.6 Particles Movement

Particles are moved using the XSPH variant (Monaghan, 1989). XSPH ensures each particle movement is consistent with the average velocity of its neighboring particles on particle distribution. In other words, the purpose of XSPH is to make fluid particle flows together with its neighboring fluid particles to make it more localized and stable.

$$\frac{d\vec{r}_a}{dt} = \vec{v}_a + \varepsilon \sum_b \frac{m_b}{\bar{\rho}_{ab}} \vec{v}_{ab} W_{ab} \quad (10)$$

where, $\varepsilon = 0.5$ and $\bar{\rho}_{ab} = (\rho_a + \rho_b)/2$. This technique moves a particle with a velocity that is close to the average velocity in its neighborhood.

2.1.1.7 Density Reinitialization

The pressure field of the particles exhibits large pressure oscillations although the dynamics from SPH simulations are generally realistic. Approaches to solve this problem includes correcting the kernel and developing an incompressible solver. One of the most straight forward and computationally least expensive is to perform a filter over the density of the particles and the re-assignment of density to each particle. There are two orders of corrections, namely the zeroth order and first order. Herein, first order of correction is applied to increase the accuracy of the obtained results (Dilts, 1999). Successfully developed moving least squares (MLS) and was applied by (Colagrossi and Landrini, 2003) and (Panizzo, 2004). This is a first order correction so that the linear variation of the density field can be exactly reproduced as:

$$\rho_a^{new} = \sum_b \rho_b W_{ab}^{MLS} = \sum_b m W_{ab}^{MLS} \quad (11)$$

The corrected kernel is evaluated as follows:

$$W_{ab}^{MLS} = W_b^{MLS}(\vec{r}_a) = \beta(\vec{r}_a) \cdot (\vec{r}_a - \vec{r}_b) W_{ab} \quad (12)$$

so that in two-dimensional space, it can be written as:

$$W_{ab}^{MLS} = [\beta_0(\vec{r}_a) + \beta_{1x}(\vec{r}_a)(x_a - x_b) + \beta_{1z}(\vec{r}_a)(z_a - z_b)] + W_{ab} \quad (13)$$

where the correction vector, $\beta(\vec{r}_a)$ is given as follows:

$$\beta(\vec{r}_a) = \begin{bmatrix} \beta_0 \\ \beta_{1x} \\ \beta_{1z} \end{bmatrix} = (\sum_b W_b(\vec{r}_a) \tilde{\mathbf{A}} V_b)^{-1} \begin{bmatrix} 1 \\ 0 \\ 0 \end{bmatrix} \quad (14)$$

with the matrix $\tilde{\mathbf{A}}$ being defined as:

$$\tilde{\mathbf{A}} = \begin{bmatrix} 1 & (x_a - x_b) & (z_a - z_b) \\ (x_a - x_b) & (x_a - x_b)^2 & (z_a - z_b)(x_a - x_b) \\ (z_a - z_b) & (x_a - x_b)(z_a - z_b) & (z_a - z_b)^2 \end{bmatrix} \quad (15)$$

The filter is applied in every 30 time steps. In the case of three-dimensions, the equations are similar but just with the addition in the y -direction.

2.1.1.8 Time Stepping

The predictor-corrector (PC) scheme described by (Monaghan, 1989) is implemented in this SPH simulation. The governing equations for this scheme are listed as follows:

$$(i) \text{ momentum equation: } \frac{d\vec{v}_a}{dt} = \vec{F}_a \quad (16)$$

$$(ii) \text{ density equation: } \frac{d\rho_a}{dt} = D_a \quad (17)$$

$$(iii) \text{ position equation: } \frac{d\vec{r}_a}{dt} = \vec{V}_a \quad (18)$$

where \vec{V}_a denotes the velocity contribution from particle a and neighboring particles based on XSPH correction.

The scheme predicts the evolution in time as,

$$\dot{\vec{v}}_a^{n+1/2} = \dot{\vec{v}}_a^{n/2} + \frac{\Delta t}{2} \vec{F}_a^n \quad (19)$$

$$\rho_a^{n+1/2} = \rho_a^{n/2} + \frac{\Delta t}{2} D_a^n \quad (20)$$

$$\dot{\vec{r}}_a^{n+1/2} = \dot{\vec{r}}_a^{n/2} + \frac{\Delta t}{2} \vec{V}_a^n \quad (21)$$

by calculating $P_a^{n+1/2} = f(P_a^{n+1/2})$ in accordance with Eq. (9).

These values are then corrected using forces at the half step

$$\dot{\vec{v}}_a^{n+1/2} = \dot{\vec{v}}_a^{n/2} + \frac{\Delta t}{2} \vec{F}_a^{n+1/2} \quad (22)$$

$$\rho_a^{n+1/2} = \rho_a^{n/2} + \frac{\Delta t}{2} D_a^{n+1/2} \quad (23)$$

$$\dot{\vec{r}}_a^{n+1/2} = \dot{\vec{r}}_a^{n/2} + \frac{\Delta t}{2} \vec{V}_a^{n+1/2} \quad (24)$$

Finally, the values are calculated at the end of the time step

$$\dot{\vec{v}}_a^{n+1} = 2\dot{\vec{v}}_a^{n+1/2} - \dot{\vec{v}}_a^n \quad (25)$$

$$\rho_a^{n+1} = 2\rho_a^{n+1/2} - \rho_a^n \quad (26)$$

$$\dot{\vec{r}}_a^{n+1} = 2\dot{\vec{r}}_a^{n+1/2} - \dot{\vec{r}}_a^n \quad (27)$$

Lastly, the pressure is computed from density using the relation:

$$P_a^{n+1/2} = f(P_a^{n+1}) \quad (28)$$

2.1.1.9 Boundary Conditions

In SPH, boundaries are described using a discrete set of boundary particles that exert a repulsive force on the fluid particles when they are approached. In the SPH model used in this work, a dynamic boundary condition is implemented (Dalrymple and Knio, 2001; Crespo, 2008). This method sees boundary particles that satisfy the same equations as fluid particles, however they do not move according to the forces exerted on them. Instead, they remain either fixed in position or move according to an imposed or assigned motion function. Fig. 1 depicts the boundary particles that are arranged in staggered manner. From the two-dimensional sketch, the fluid particle is described as blue outline dot whereas the boundary particles are represented by black solid dots. Under this boundary condition, when a fluid particle approaches a boundary particle and the distance between them decreases beyond the kernel range, the density of the affected boundary particles increases, giving rise to an increase in pressure. This in turn results in a repulsive force being exerted on the fluid particle due to the pressure term, P/ρ^2 in the momentum equation.

Periodic boundary condition is the phenomena where the f_i leaves the flow domain and subsequently will re-enter on the opposite side. For current SPH numerical model of stepped spillway, periodic boundary condition will be applied on both the

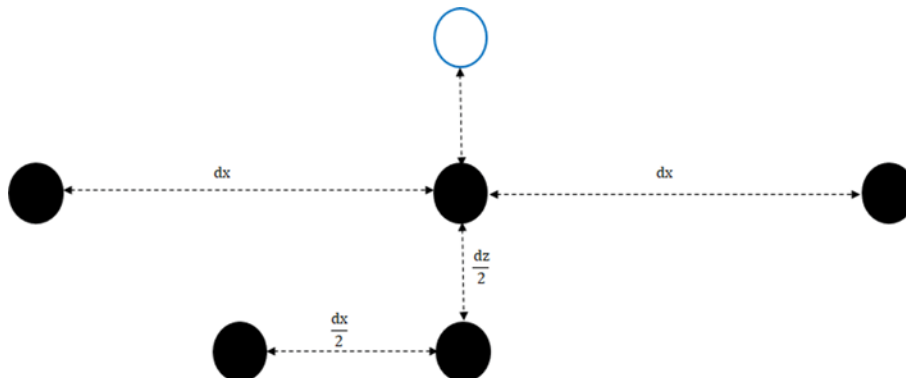


Fig. 1. Interaction between a Fluid Particle (blue outline) and a Set of Boundary Particles (solid black)

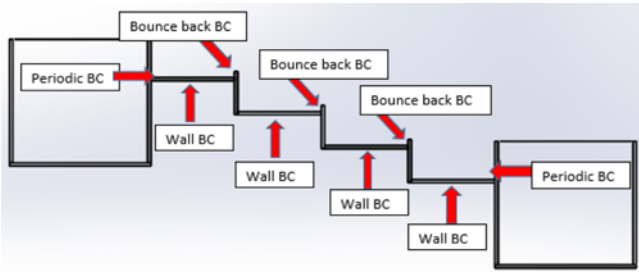


Fig. 2. Periodic, Bounce Back and Wall Boundary Conditions as Imposed on the Stepped Spillway Model in the SPH Numerical Study

model’s inlet and outlet. Besides, bounce back boundary condition is set at the vicinity of each barrier of stepped spillway; whereas the no-slip wall boundary is adopted elsewhere, such that the wall of the step. All these described boundary conditions as applied on

the stepped spillway are labeled on the stepped spillway model in Fig. 2.

2.1.1.10 Real Model SPH Setup

In this paper, a total of two stepped spillway models of different barrier heights are being investigated. The height of the barrier for each stepped spillway model, d are 10 mm and 25 mm in Case 1 and Case 2, respectively. In terms of the geometry, the stepped spillway in both test cases are similar, which consists of four identical steps that are connected to a reservoir tank in which the water flows from it. A collector tank is then placed at the end of the flow as being illustrated in Fig. 3.

The stepped spillway models described in both Case 1 and Case 2 are generated using an open-source SPH software (Monaghan, 1989; Dilts, 1999; Monaghan, 1992; Colagrossi and Landrini, 2003; Panizzo, 2004; Crespo, 2008). The stepped

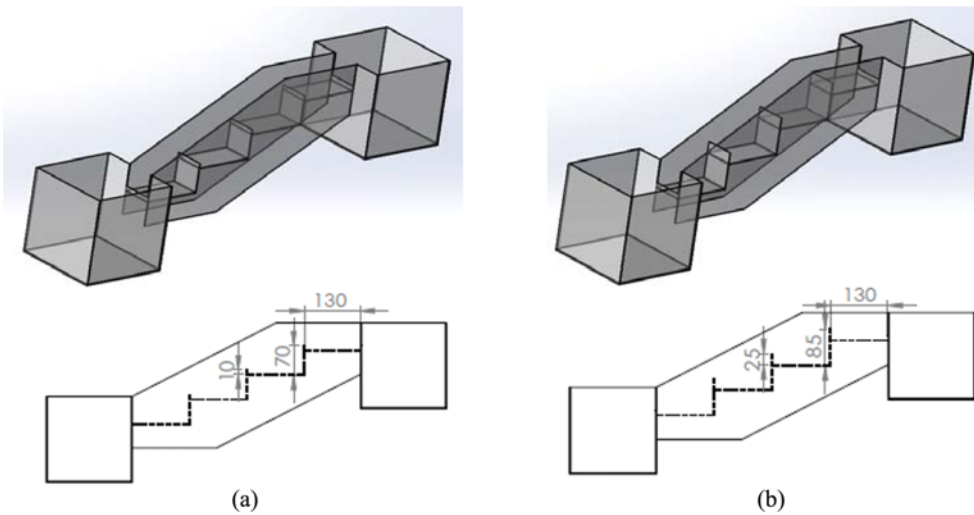


Fig. 3. Design of Stepped Spillway with Its Detailed Dimensions for Both Configurations in: (a) Case 1, (b) Case 2

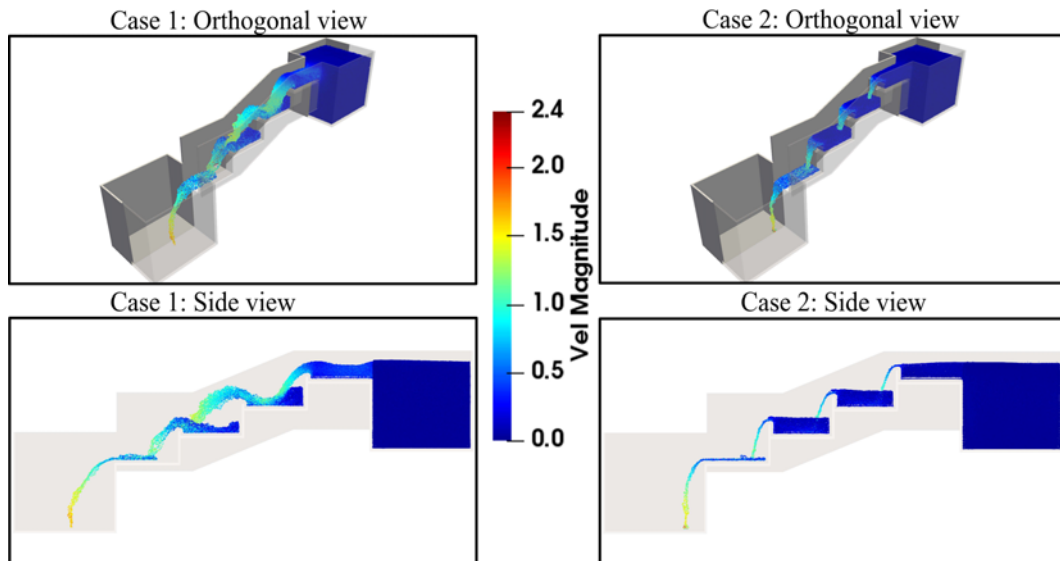


Fig. 4. Steady Water Flows along the Stepped Spillway Models in Case 1 and Case 2, as Viewed Orthogonally and from Side, Respectively

spillway structure, reservoir tank and water are modelled into finite particles.

Figure 4 shows both the orthogonal and side views of the stepped spillways models in both Case 1 and Case 2. To optimize both the precision and computational cost, the number of particles in the simulation is optimized by considering a narrow width of the jet stream of 68 mm that is similar to the width of the reservoir's outlet. This approach is valid as the water flowing down the stepped spillway are symmetrical in that direction. Accordingly, the analysis and visualization of water flow along the stepped spillway in the forthcoming sections are generally in accordance to its side view observations.

2.1.2 Distance Particle Analysis

Figure 5 shows the distance particle (dp) analysis for the model in order to achieve highest accuracy and precision. The graph shows the line pattern between four different dp values of 0.01, 0.005, 0.0025 and 0.001. The trend lines for 0.005, 0.0025 and 0.001 were shown to be almost similar to each other as compared to the biggest particle spacing of 0.01. This means that all dp managed to capture the velocity overall behavior of the flow across the time span, however, two dp value of 0.0025 and 0.001 were shown to be nearly identical in terms of trend and fluctuations. To optimize between accuracy and computation time, the dp value of 0.0025 is chosen to the model due to its relatively lower computation time while still achieving high accuracy in the computed velocity values as compared to dp of 0.001.

2.2 Particle Image Velocimetry

This section describes the PIV experiment that is being conducted to validate the findings from SPH numerical models. Exact dimensions of the stepped spillway models for both configurations in Case 1 and Case 2 are used in the PIV setup that are identical to that being adopted in SPH, with its dimensions being given in Fig. 4. These stepped spillway models are fabricated using clear Perspex of thickness 5 mm.

Generally, PIV is an optical method used to identify

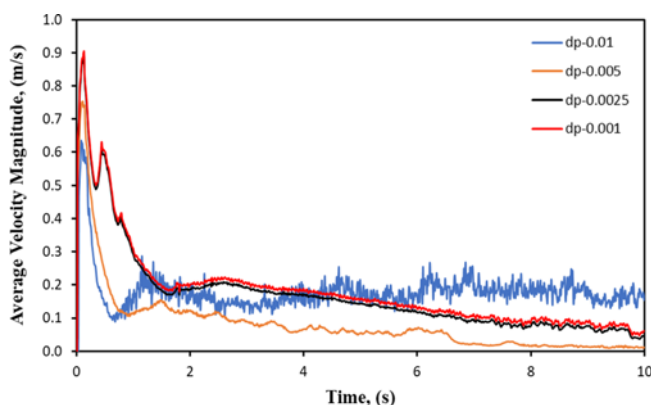


Fig. 5. Distance Particles Analysis for Average Velocity along Period of 10s

instantaneous vector field in a cross-sectional fluid flow. The velocity field can be determined based on the movement of the tracer particles that are being introduced to the flow. The tracer particles are illuminated at two-time instances that are subsequently being recorded using a camera. Since the time interval between the two light pulses are known, the magnitude and direction of the particles group can be determined. PIV translates the continuum Eulerian flow into particle Lagrangian approach to visualize the flow dynamics especially its velocity vector.

The measurement of the velocity fields of the river bank model is performed using a PIV system that consist of the integration of an illumination setup, an imaging device and a personal computer. The illumination in PIV system is achieved by using a combination of high-powered light emitting diode (LED) that diverges from cylindrical lens and fibre optic bundle as shown in Fig. 6. Thin light sheet produced is illuminated perpendicularly from the bottom of stepped spillway to prevent refraction that may distorts the collimated illumination beam.

Furthermore, considerable amount of 50 μm polyamide seeding particles is mixed evenly with water before added into the reservoir. It serves as the tracking particle for water flow in the PIV system for determination of flow's velocity vector. Additionally, progressive scan interline CCD camera is used to record the water flow. Generally, the complete PIV experimental setups for both configuration in Case 1 and Case 2 are depicted in Fig. 7.

During the experiment, water is pumped from the lower reservoir to the upper reservoir. While the water level in the

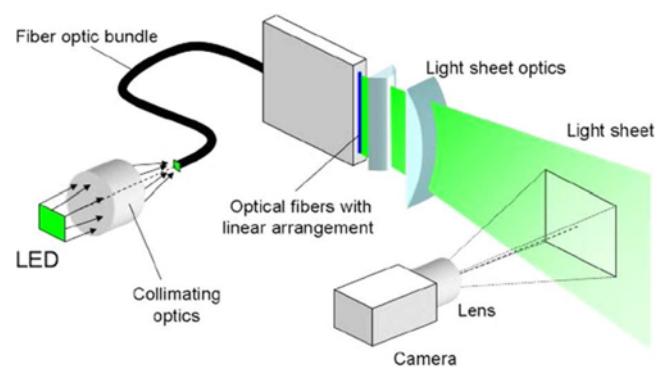


Fig. 6. LED-Based Illumination Setup in PIV System

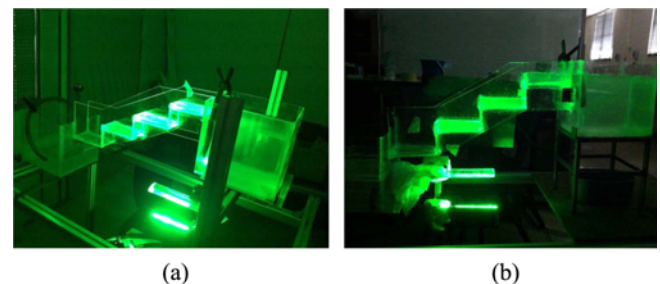


Fig. 7. Actual PIV Experimental Setups of Stepped Spillways with Different Barrier's Heights: (a) $d = 10$ mm in Case 1, (b) $d = 25$ mm in Case 2

upper reservoir is higher than the reservoir gate, the pressure difference enable it to gradually flow down the steps. The water flow rate is set to be constant at $2.69 \times 10^{-4} \text{ m}^3/\text{s}$. To minimize the transient effects that may arise during the water flow at the early stage, all measurements were taken five minutes prior to the pump start up. Subsequently, the images captured will be processed jointly using IC Capture and PIVlab software to obtain the desired velocity vectors of the flow along the stepped spillway models.

2.3 Principal of Energy Dissipation and Aeration Efficiency of Flows

The aeration process in the stepped spillway is based on the local phenomenon of hydraulic jump that occurred near the barrier at the end of each step. Fig. 8 generally summarized the mechanisms of the hydraulic jump with its flow characteristic. It is found that the region near the occurrence of hydraulic jump exhibits highly turbulent flow while the flow vortices formed dissipated kinetic energy in the flow itself.

During the occurrence of hydraulic jump, the free surface of flow abruptly increases with a strong agitation and substantial amount of energy loss that is equivalent to the head loss, ΔH which given as:

$$\Delta H = \left(d_1 + \frac{U_1^2}{2g} \right) - \left(d_2 + \frac{U_2^2}{2g} \right) \quad (29)$$

In which, d is the height from datum, U is the flow's velocity and g is the gravitational acceleration. The subscripts "1" and "2" refer to the flow's parameters before and after the hydraulic jumps, respectively. Meanwhile, the rate of energy dissipated per unit channel width of the flow after hydraulic jump is:

$$\omega = \dot{q} \Delta H \gamma \quad (30)$$

with the mass flow rate per unit channel $\dot{q} = 0.03 \text{ m}^2/\text{s}$ and the specify gravity of water at ambient condition (1 atm, 25°C), $\gamma = 95843 \text{ N/m}^3$. Subsequently based on the extensive experimental data collected, the positive linear relationship between the aeration efficiency, η and rate of energy dissipation, ω is found. The correlation equation of best-fitting line is determined as (Chanson and Toombes, 2002):

$$\eta = 0.0015 \omega + 0.01 \quad (31)$$

Theoretically, it is observed that the aeration efficiency is

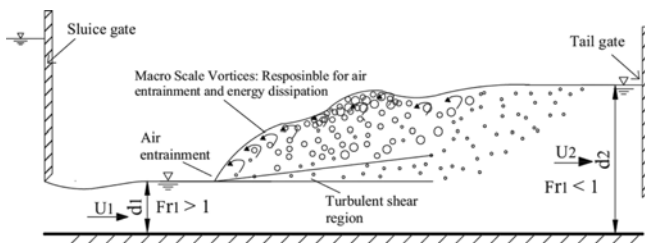


Fig. 8. Schematic Illustration of Typical Hydraulic Jump and Its Flow Characteristics (The fluid flows from sluice gate and approaching the tail gate (Chanson and Toombes, 2002))

directly proportional to the head loss and thus the energy dissipation rate. High aeration efficiency implied that more oxygen will be dissolved into the water during the hydraulic jump if more vigorous vortices are being formed in the flow. A more prominent turbulent flow is observed in the flow regime that is closely related to the higher power dissipation in the flow and larger head loss (Gonzalez and Chanson, 2007).

Quantitative analysis of the aeration energy dissipation based on SPH simulation data reveals that the energy is being dissipated that gradually increases over the steps. The results obtained are in good agreement with the theoretical background studied. Energy dissipation can be achieved by breaking the falling jet in the air and subsequently the jet mixing on the steps. Also, the presence of an isolated stilling basin or barrier at the edge of each step acts an energy dissipater to reduce the energy by converting the kinetic energy of flow into turbulence vortices. It is also noted that the turbulence may be observed as the swirling of water within the cavity. Besides, the formation of hydraulic jump will further enhance the dissipation of the excess energy. In the case of aeration performance, it has been noticed that variation in aeration efficiency over the steps does show positive results.

2.4 Dimensionless Analysis

Generally, the flow dynamic of water in the stepped spillway model is mainly characterized by its velocity, which can be expressed as the function of fundamental parameters of the spillway:

$$U = f(\rho, \mu, h, H, L, g) \quad (32)$$

Through dimensionless analysis, the dimensionless terms associated to the flow in stepped spillway are obtained as follows:

(i) Aspect ratio of weir height to step height:

$$h^* = \frac{h}{H} \quad (33)$$

(ii) Reynold number, forces ratio of inertia to viscous:

$$\text{Re} = \frac{\rho U h}{\mu} \quad (34)$$

(iii) Froude number, forces ratio of inertia to gravitation:

$$\text{Fr} = \frac{U}{\sqrt{gh}} \quad (35)$$

The dimensionless aspect ratio in (i) denotes the geometrical similarity of the scaling aspect of stepped spillway model; while subsequent dimensionless numbers (ii) and (iii) provided the dynamic similarity aspect as the forces ratio between two dominate force in the flow. From the dynamic dimensionless numbers, the characteristic flow velocities are obtained as follows:

$$U_{Re} = \frac{\mu}{\rho h} \quad (36)$$

$$U_{Fr} = \sqrt{gh} \quad (37)$$

For water (at 25°C) with density $\rho = 997 \text{ kg/m}^3$, dynamic

viscosity $\mu = 8.90 \times 10^{-4}$ Pa-s, the characteristic velocities at stepped spillway with $h = 10$ mm are respectively computed as $U_{Re} = 8.927 \times 10^{-5}$ m/s and $U_{Fr} = 0.313$ m/s. With $U_{Re} \ll U_{Fr}$, and from numerical observation that $U \sim 1$ m/s, it can be concluded that both the inertia force and gravitational force are similar order of magnitude and dominating over the viscous term. As a result, the Reynold number of flows would have order of magnitude ranging from $10^2 - 10^5$, giving the flow exhibits prominent turbulent nature with slight laminar and transition flow regimes. For the scaling aspect, the actual flow velocity in actual scale model of stepped spillway, U_o , can be determined by matching the Froude number as follows:

$$\frac{U_o}{\sqrt{h_o}} = \frac{U_s}{\sqrt{h_s}} \Rightarrow U_o = \frac{1}{\sqrt{f_s}} U_s \quad (38)$$

In which, U_s is the velocity of scaled-model with the scaling factor, f_s relative to the original model. The current scaled-down model would predict smaller velocity by a factor of $\frac{1}{\sqrt{f_s}}$. This is in accordance to the fact when the water falls from one step to lower step, the gravity accelerates the flow and larger step distance would increase the flow velocity.

3. Results and Discussions

3.1 Visual Observation of Water Flow along Stepped Spillway Simulated Using SPH

For both stepped spillway models in Case 1 and Case 2, the water that is being accumulated in the reservoir will flows through the inlet and gradually descends down the steps by converting gravitational potential energy to kinetic energy of the flow. Part of the energy may loss as sound and heat while flows through the stepped spillway as well as due to the phenomenon of hydraulic jump. During the aeration process, macro vortices is formed with part of the energy being dissipated causing the oxygen to be gradually dissolved in the water as it is exposed to the environment. Subsequently, this will enhance its quality of aeration.

The side view of water flow along each steps Figs. 11(a) – 11(d) on the spillway models as being compared in both configurations of Case 1 and Case 2 are presented in Fig. 11. As the main difference between the both configurations are the height of the barrier, therefore flows as being visualized in Fig.

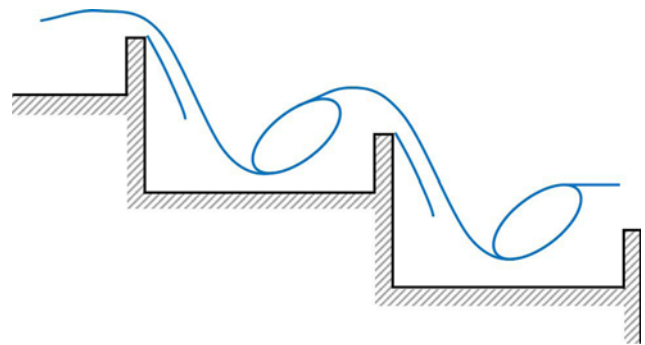


Fig. 9. Illustration of Free-Falling Flow over Pooled Stepped Spillway

11 are almost identical and exhibit a nappe flow regime with typical flow patterns for free-falling jets as it moves from higher step to the lower step as depicted in Fig. 9. It is noteworthy that the occurrence of swirling and water splashing particularly at the seconds steps onward are more prominent in Case 2 upon close comparison to Case 1.

In general, there are three common types of flows that is can be found in the stepped spillway, namely the nappe, transition and skimming flows as illustrated in Fig. 10. Nappe flow usually happens at low flow rates and longs steps relative to its height. On the contrary, skimming flow occurs at larger flow rates in which the water flows down the stepped face as a coherent stream. Transition flow is the flow regime which is situated in the region between these two flows.

The flow pattern on stepped spillway is strongly associated with the dimension and design of the spillway itself together with the water flow rate. Since other parameters in both spillway setups are kept constant, the slight increase of barrier's height from 10 mm to 25 mm does not significantly alter the general flow pattern along the stepped spillway. This is inferred based on the previous observation that both configurations of Case 1 and Case 2 exhibited qualitative similar napped flow pattern.

3.2 Validation of SPH Models Using PIV Experiment

Figure 12 depicts the velocity vector of water flows along the stepped spillway in both configurations. Generally, for the flow in Case 1, the water proceeds in a series of plunges from one step to the other. The flow from each step hits the step below as a falling jet with the energy dissipation occurring due to jet breakup on the air, jet mixing on the step and the formation of a

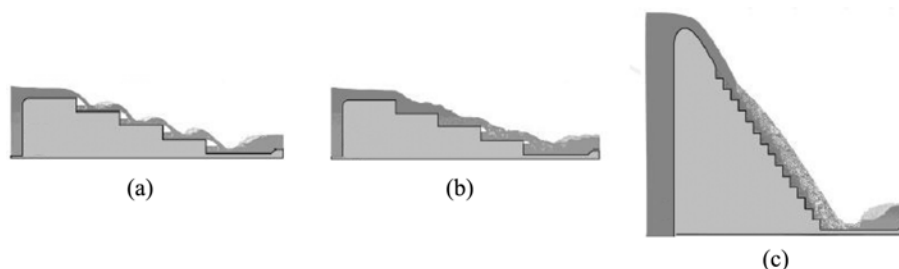


Fig. 10. Flow Pattern on Stepped Spillway: (a) Nappe Flow, (b) Transition Flow, (c) Skimming Flow

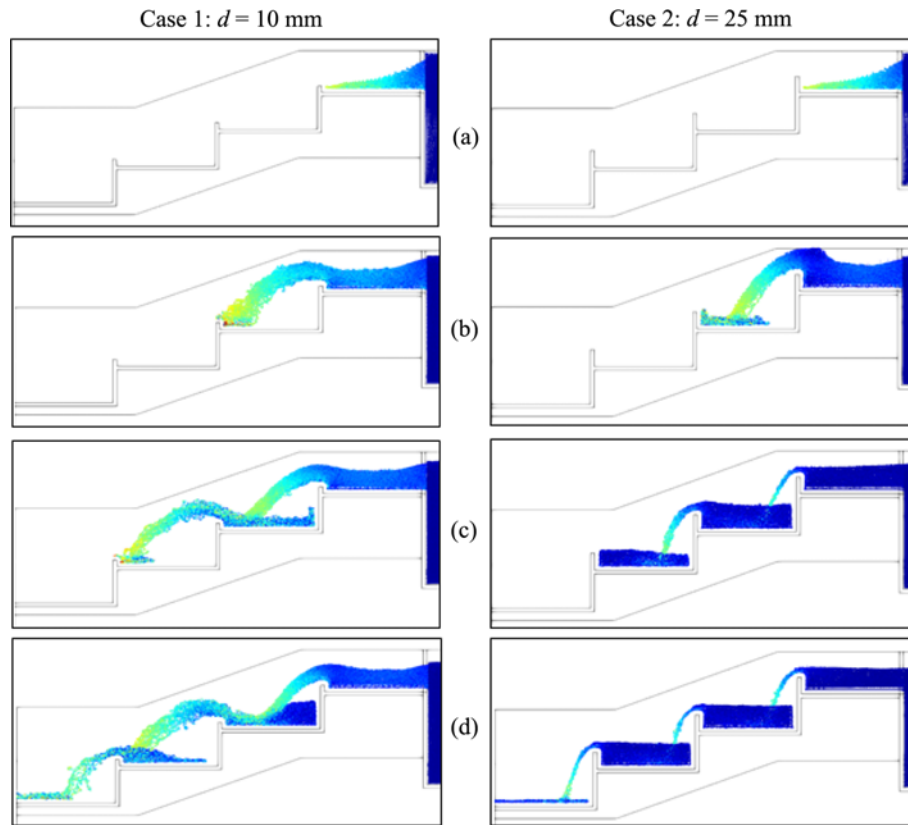


Fig. 11. The Particulate Water Flow Simulated by SPH in Both Stepped Spillway Models as Described in Case 1 and Case 2, as the Flow Progress from: (a) First Step, (b) Second Step, (c) Third Step, (d) Fourth Step

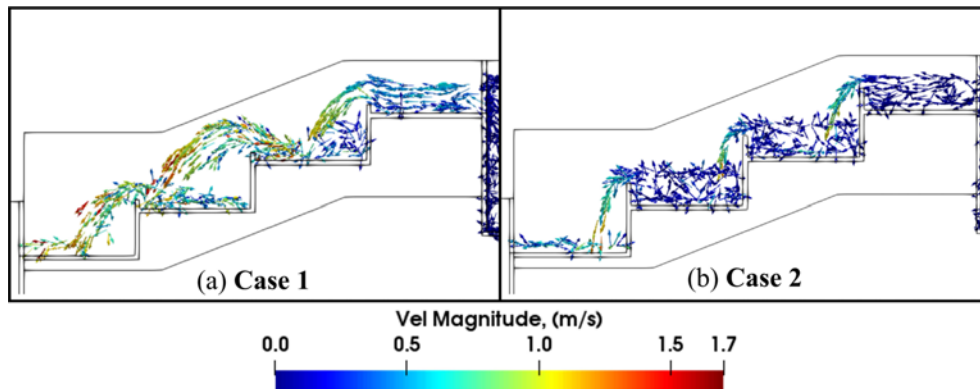


Fig. 12. The Velocity Vector Distributions of Steady Water Flow along the Stepped Spillway Models as Described in: (a) Case 1, (b) Case 2

hydraulic jump on the edge of step. Overall, the velocity vectors of flow depicted in Case 1 are more uniform and well-ordered implying a laminar flow along the stepped spillway. The main difference as being noticed in Case 2 is that there are obvious swirling of water and vortices that is associated with turbulent flow regime being formed at the vicinity of the second and third steps. Furthermore, it is also noticed that the overall velocity magnitude is higher for the water flow in Case 2 than in Case 1.

The flow’s velocity vectors at first, second and third steps of the stepped spillways for both configurations in Fig. 12 are analyzed to be compared with the flow vectors attained from PIV experiment at similar locations and setups. Side-by-side comparison

between SPH simulation flow pattern with the corresponding PIV experimental results are presented in Fig. 13 with the flow regime characteristics that include laminar, transition or turbulence are being studied. In general, it is found that the flow pattern in the numerical SPH models along the stepped spillway models in both cases are comparable to the flow profiles attained using experimental PIV method for all three steps. This subsequently affirmed the validity of our numerical SPH models.

Major similarity between SPH and PIV flow patterns and behaviors are particularly emphasized in the dashed boxes in Fig. 13. The orange-colored outline box in Fig. 13 depicts laminar flow that is characterized by the presence of smooth streamlines.

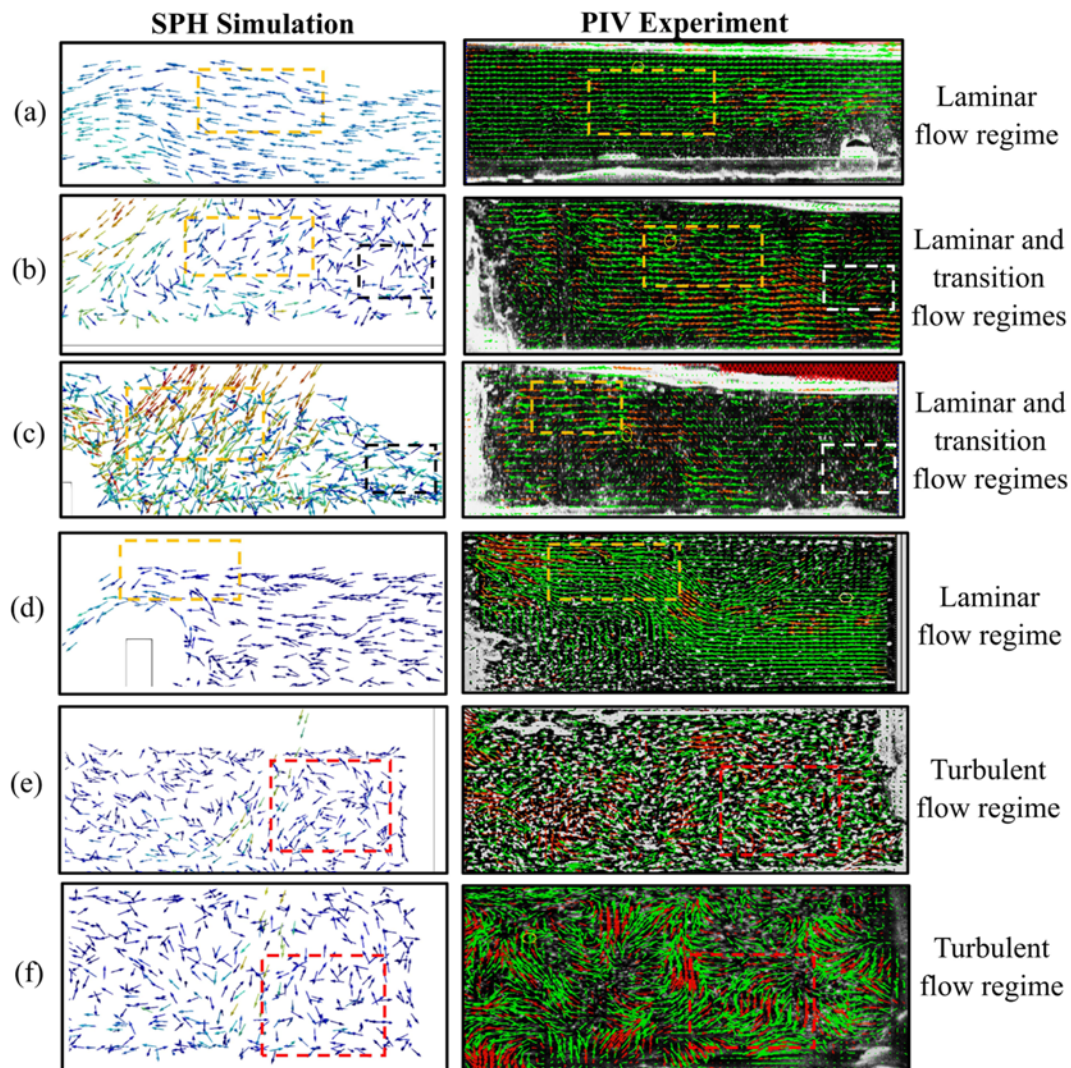


Fig. 13. Comparison of SPH Water Flow with Experimental PIV at Different Steps of the Stepped Spillway Models for Case 1: (a) First Step, (b) Second Step, (c) Third Step; while Case 2: (d) First Step, (e) Second Step, (f) Third Step (Note: The orange box highlighted the similar laminar flow regime that observed in both SPH and PIV, whereas red box for turbulence flow regime and white-black box for transitions regime.)

These streamlines exhibit highly ordered motion and possess low Reynolds number. All the three steps in the stepped spillway of Case 1 resides in laminar flow regime that is similar to first step in Case 2. On the other hand, some turbulent flows are observed at the step cavity as a result of the actions of jet breaking followed by jet mixing. Turbulent flow is characterized by the velocity fluctuation and highly disordered motion with high Reynolds number. The flow patterns comparison between both configurations revealed that the occurrence of water turbulence is more likely in the stepped spillway of Case 2. Based on Fig. 13, water turbulence and macro-scale vortices are observed as the swirling of water as indicated by red-colored outline box is mainly observed in the second and third steps of Case 2. It is worth to mention that there is a possibility for the development of potential vortices and mild water swirling (white-colored outline box) at the cavity near the second and third steps of Case 1. However, due to the relatively lower flow velocity and

considerably uniform flow, turbulence flow is not formed in this region. Therefore, these may be regarded as the transition flow regime, for which its Reynolds number is in between that of laminar flow and turbulence flow.

In fact, this great consensus obtained between both SPH simulation and PIV experiment findings are mainly contributed to their common theoretical approach – Lagrangian particle method. Both the Eulerian continuum flow and stepped spillway are being modelled as finite particles in the SPH simulation. Meanwhile fine particles are added to the water flow, to be used for tracking of the water flow based on imaging technique using in the PIV method.

3.3 Points of Interest on the Stepped Spillway Models

Five points of interest have been chosen based on the visualization of flow behaviors in Sections 4.1 and 4.2 with probes placed at points *P*, *Q*, *R*, *S* and *T* along the stepped spillway. These points

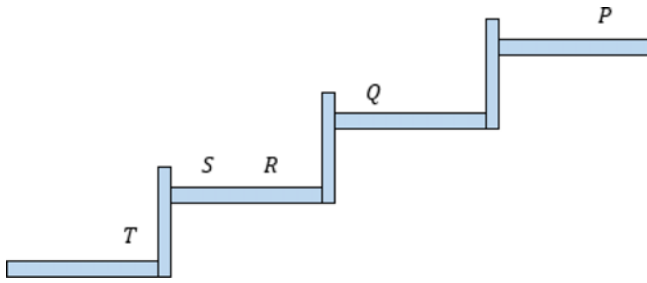


Fig. 14. Approximate Locations of the Five Points of Interest (*P*, *Q*, *R*, *S* and *T*) on the Stepped Spillway Models, Valid for Both Case 1 and Case 2

Table 1. Explanations for the Selection of Points of Interest (*P*, *Q*, *R*, *S* and *T*) along the Stepped Spillway

Point(s)	Explanation
<i>P</i>	Laminar flow from the reservoir’s outlet that will served as the inlet flow to the stepped spillway.
<i>Q</i> and <i>S</i>	Vicinity of the occurrence of hydraulic jump and aeration process.
<i>R</i> and <i>T</i>	Potential region of highly occurrence of vortices, swirling and turbulence.

are similar and applicable for both stepped spillway models in Case 1 and Case 2 are being illustrated in Fig. 14. These will simplify the explanation for validation done in the subsequent sections, particularly on flow’s velocity, pressure and aeration efficiency. The fundamental reasons for selection these five points for discussion purposes are summarized in Table 1. This will also ensure there is at least one point being selected at each step.

3.4 Velocity Distribution of Water Flow in Stepped Spillway

Both experimental and simulation magnitude of flow velocities at selected point of interest, *P*, *Q*, *R*, *S* and *T*, for stepped spillway models of both cases are presented in Fig. 15. It is observed that the velocity of water increases as its flow progresses along the stepped spillways for both models. This constitute for the energy conversion as the gravitational potential energy gradually being converted into kinetic energy of flow. Part of this energy may be loss as heat and sound through rough wall of stepped spillway as well as due to hydraulic jump that will be covered in the subsequent section. For Case 1, higher flow velocity is observed at points *R* and *S* in comparison to Case 2. In contrast lower velocity is shown at points *P*, *Q* and *T*. Additional analysis shows that the average velocity at these five points based on SPH models in Case 1 and Case 2 are 0.302 m/s and 0.316 m/s, respectively. This shows that the flow in Case 2 is slightly faster than that in Case 1.

In fact, both PIV experiment and SPH simulation gave quite similar values of flow velocity at those selected points. This again serves as a good validation to our numerical models as a whole in addition to the visual comparison of flow as being

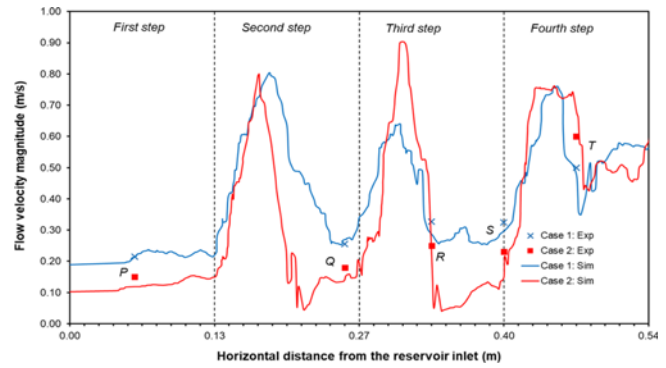


Fig. 15. Comparison of Flow’s Velocity Obtained in SPH Simulation and PIV Experiment at Selected Points on Stepped Spillway Models for Case 1 and Case 2

present in Section 4.2 earlier. Highest deviation is however being noticed at point *S* whereas the least deviation found at point *R*. Still, the overall trend based on the numerical simulation agree wells with the experimental finding with the overall average velocity deviation of about 10.78%.

Visual observation of the velocity distributions of water flow at each step in two different stepped configurations – Case 1 and Case 2 are presented in Fig. 16. This figure aims to investigate the changes in flow patterns at different steps for both models. For both configurations, a nappe flow regime existed that exhibits typical flow patterns with falling jets from one step to the other. Nevertheless, Case 2 exhibits some small instabilities linked with slightly more splashing or swirling of water in the flow regime upon comparison with Case 1. Based on the flow time given in Fig. 16, it is inferred that the water flow is slightly accelerating prior to flowing down the steps due to gravity and inlet pressure at the reservoir. This is evident in the increase of flow velocity at the lower steps as seen in Fig. 15.

Moreover, the discrepancy between the flow velocity distributions in both configurations are found to be minimal based on the visual observation of particulate flow. Through quantitative analysis, it appears that Case 2 experienced slightly faster flow due to falling jet of water from a higher elevation as the barrier height has been increased. It took 0.77 s and 2.26 s for the water to reach the fourth steps of the stepped spillway in Case 1 and Case 2, respectively. Further, it is noticed that the velocity of the flow as it just passes over the barrier is the highest compared to other region at a particular step and elevation.

3.5 Pressure Distribution of Water Flow in Stepped Spillway

The gauge pressure variations at selected points *P*, *Q*, *R*, *S* and *T* on stepped spillway in Case 1 and Case 2 are depicted in Fig. 17. For all cases, it is found that the pressure of the water decreases as it descends along the stepped spillway models. Careful observation shows that the pressures at points *P*, *Q* and *T* are higher for Case 1 compared to Case 2 in contrast to the readings found at points *R* and *S*. Additionally, the average total pressure of flow over these five points in Case 1 and Case 2 are 3039 Pa

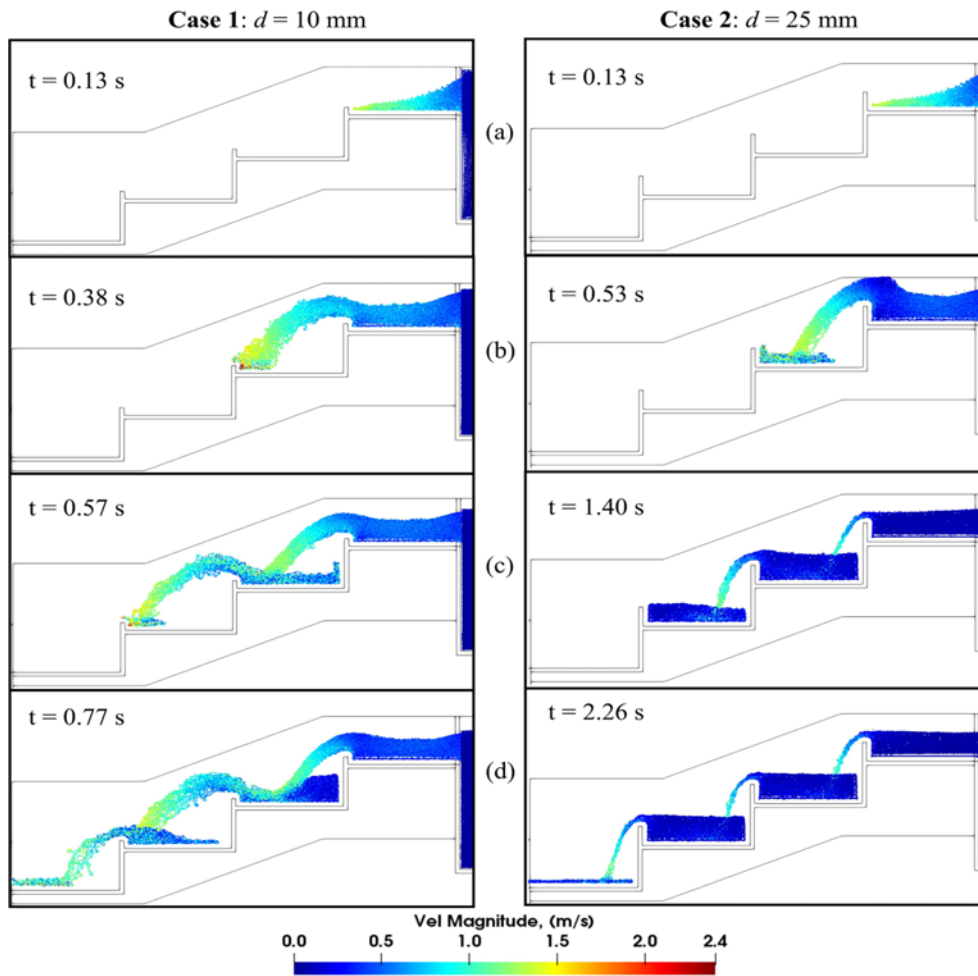


Fig. 16. Comparison of Velocity Distribution of Water Flow between the Stepped Spillway Models in Case 1 and Case 2, as the Flow Progress from: (a) First Step, (b) Second Step, (c) Third Step, (d) Fourth Step with Time, t

and 2659 Pa, respectively indicating a more pressurized flow found in Case 1. These findings complement the flow velocity trend as previously argued in Section 3.4 that is in accordance to the Bernoulli principle. It is stated that for flow in a closed system without external influences, the stagnant pressure is inversely proportional to its velocity. Thus, it is inferred that both the velocity and pressure variations in both stepped spillway models were validated by cross-referencing each other and have been found to adhere to the theoretical formulation of the Bernoulli principle.

It is worth-mentioned that the negative gauge pressure only observed at point T for both cases, while the other four points recorded positive gauge pressure. Such lower than atmospheric pressure at point T is expected since there has been a substantial decline of pressure over each step. Subsequently, this huge drop in pressure relative to the previous point S located on the third step may cause the stepped spillway models to much prone to the occurrence of cavitation that can leads to prominent hydraulic jump phenomenon.

Apart from the contribution of conservation law on this declining trend in pressure, it is also partly caused by the aeration

process. As the flows progresses, the spillway design allows more oxygen to be dissolved into the water. As a result, the oxygen concentration and the partial pressure of oxygen in the flow would increase, but the partial pressure of water itself would drops. While the changes in oxygen concentration of water during the aeration process might not be significant in these first four steps, the decreases in water flow pressure due to this aeration phenomenon is not prominent.

Figure 17 depicts the pressure distributions at each step in two different stepped spillway models in both Case 1 and Case 2. It is found that the pressure at free surface of the stepped spillway models is initially equal to the atmospheric pressure of 0 Pa but substantially rises as the water flow reached that free surface. This statics pressure development is associated with the impulsive force produced during the inelastic collision of water stream and stationary surface of the spillway. In accordance to Newton's third law of action-reaction, the pressure of the water near the free surface of the steps also registered similar high-pressure trend. In contrast, the lowest pressure is being recorded for the water stream just over the barrier at the edge of each steps, such that it is lower than the atmospheric pressure. This generally

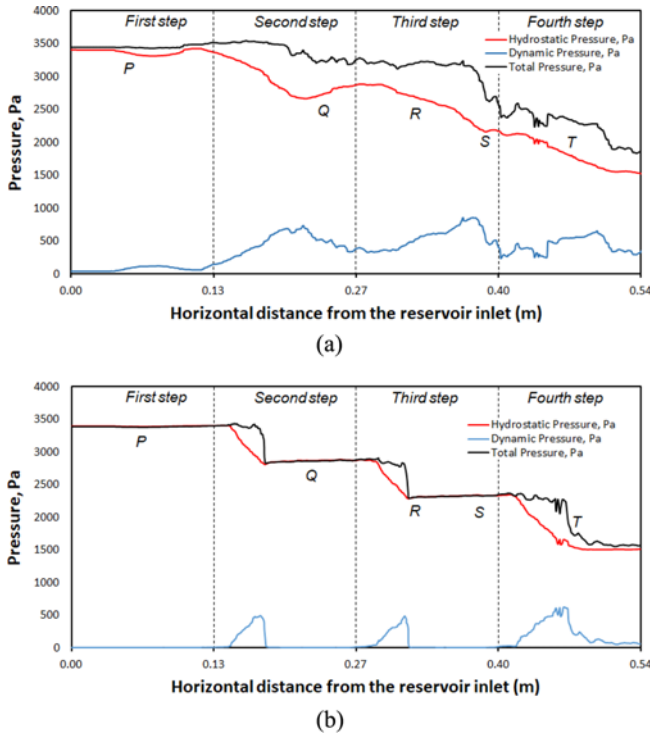


Fig. 17. SPH Simulation Pressure of Flow at Horizontal Distance at Stepped Spillway Models for: (a) Case 1, (b) Case 2

accounts for the occurrence of hydraulic jump and high velocity flow at that the vicinity of the stepped spillway’s barrier. Moreover, the turbulent regime found at points *S* and *T* for second and third steps in Case 2 possess a wide range of velocities with the fastest flow found near the free surface that will lead to the formation of vortices.

The quantitative representation as provided in Fig. 18 suggested the water flow pressure in Case 1 spreads over a larger range upon comparison with Case 2. The ranges of total pressure of the flow span from 1,500 Pa to 5,000 Pa. Higher upper limits in Case 1 is due to the overall slower water flows. Higher lower limit is shown in Case 2 is generally caused by formation of turbulence regime which substantially increases its dynamic pressure. In fact, the pressure values at five selected points in both configuration that is being presented in Fig. 17 were extracted from the flow distribution as depicted in Fig. 18. Therefore, Fig. 18 gives a clear picture on the description of the pressure variation at each points of the water flow while Fig. 17 is show a good indication of the flow behavior at points of interest.

3.6 Reynold Number Distribution of Water Flow in Stepped Spillway

Figure 19 shows the Reynold’s numbers for Case 1 and Case 2, respectively. Based on (ANSYS Inc., 2006), turbulence for an

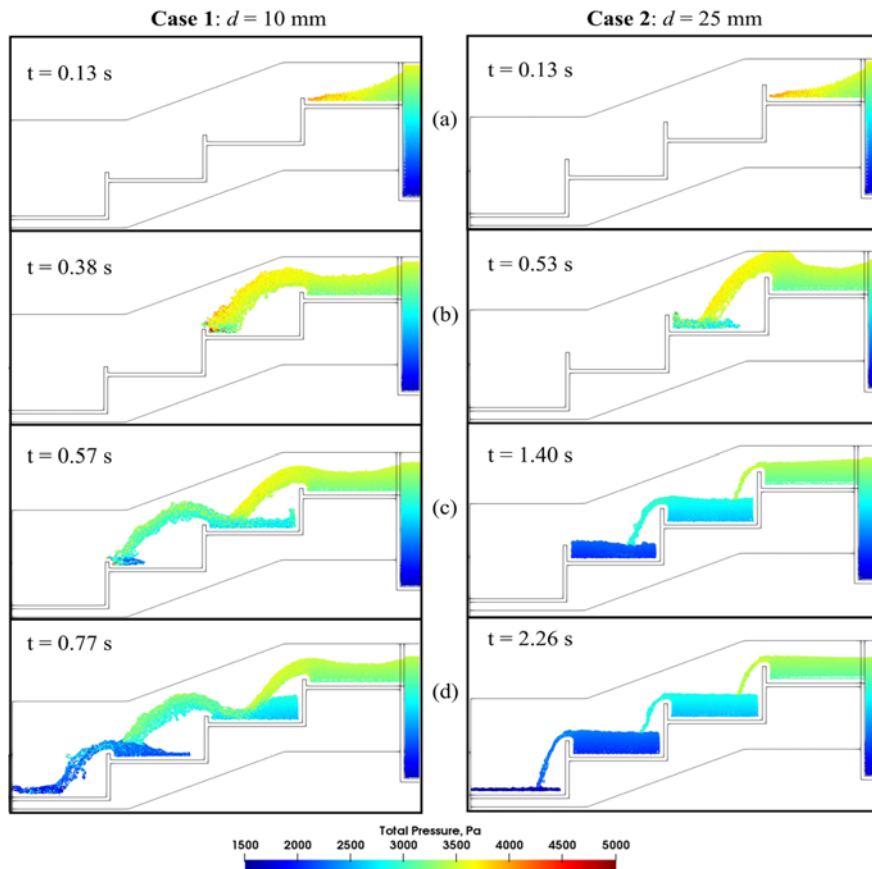


Fig. 18. Comparison of Total Pressure, Pa Distribution of Water Flow between the Stepped Spillway Models for Case 1 and Case 2, as the Flow Progress from: (a) First Step, (b) Second Step, (c) Third Step, (d) Fourth Step with Time, t

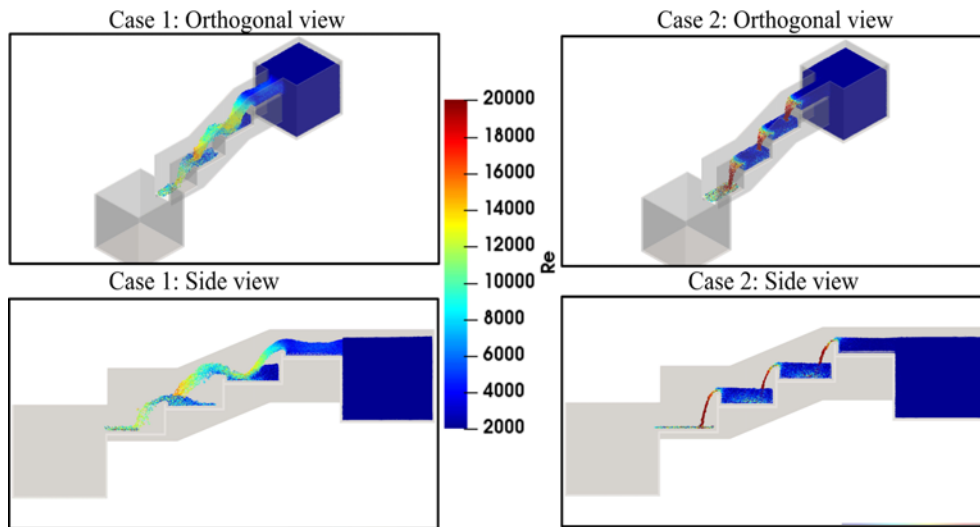


Fig. 19. Reynold's Numbers, Re along the Stepped Spillway Models in Case 1 and Case 2, as Viewed Orthogonally and from Side, Respectively

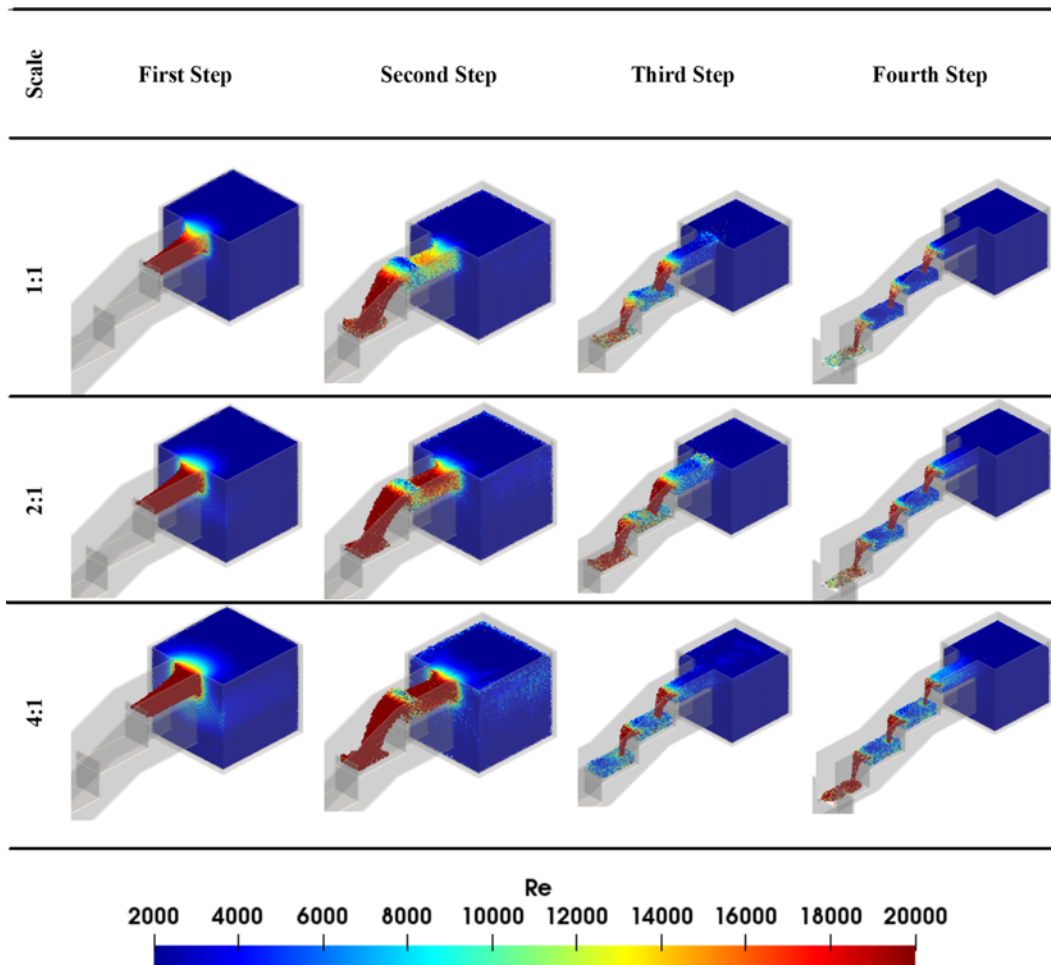


Fig. 20. Comparison of 25 mm Barrier Height (1:1) with Scale up Dimension with Reynold Number

obstacle occurs at $Re > 20,000$. Therefore, Case 2 produced high turbulence flow as compared to Case 1 whereby the turbulence flows are needed to promote air circulation which in turn

promotes the formation of manganese and iron oxides.

Figure 20 shows that the comparison of real scale (25 mm barrier height) with scale up 2:1 and 4:1. The range is set between

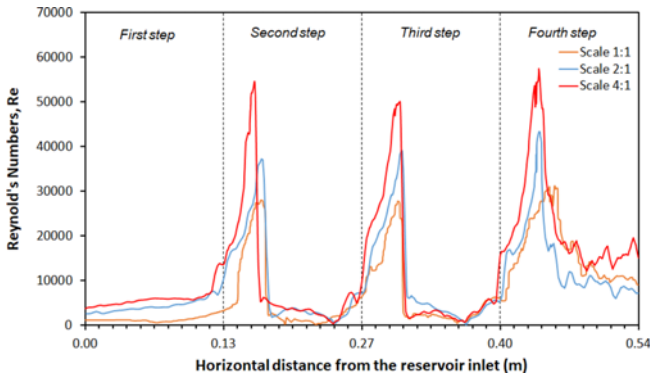


Fig. 21. Reynold Number Distribution along the Horizontal Distance from the Reservoir Inlet

2000 and 20000 which mean that the Reynold’s numbers (Re) beyond the value of 20000 will considered as turbulence flow (Twort et al., 2000; ANSYS Inc., 2006). Re pattern shows similarity between the three model 1:1, 2:1 and 4:1. The detail of comparison Re with the three model can be observed from Fig. 21.

Figure 21 shows the comparison of three model through Re with slightly similar pattern of the trend lines observed. This means that the 1:1 scale can be used to model the higher scale model for the case of flow dynamic similarity. The three peaks from Fig. 21 represents the higher Re occurs after the peak of the barrier height because at the peak of the barrier height the velocities will decreases due to higher potential energy and afterwards the velocities will increase due to high kinetic energy.

3.7 Energy Dissipation and Aeration Efficiency of Flows Due to Hydraulic Jump

Figure 22 presented the data of head loss, power dissipated and aeration efficiency of the water flow at each different steps of stepped spillways models of Case 1 and Case 2. It is found that all the variables increase with the number of steps that the water flow progress. Generally, this observation is valid for both cases. Furthermore, the head loss, power dissipated and aeration efficiency at third step is substantially much higher compared to those in first and second steps for which their values are much closer to each other. This is caused by the increases in velocity and the decreases in pressure when the flows descend the stepped spillway. These conditions will aid the hydraulic jump in aerating the water. As the water flows along the steps, the time of exposure to the external environment has been increased to allow more diffusion of oxygen into the flow. Thus, the aeration efficiency increases with more oxygen content in the flow.

Aeration efficiency is one of the crucial parameters to be considered upon quantifying the quality of the aerated water in the filtration system as well as the overall performance of the cascade aerator. The quality of water is usually indicated by the amount of dissolved oxygen content in water. The gradually increasing trend in the aeration efficiency over the steps as shown in Fig. 22 implied that there is substantial air entrainment in water due to the occurrence of turbulence mixing as the flow advances down the stepped spillway. Air entrainment is usually characterized by the entrained bubbles or droplets and several bubble or droplet clusters are observed during the experiment. Thus, the rising in aeration efficiency served as a compelling indicator that is associated to the increase in the concentration of dissolved oxygen in the water. This in turn improves the quality

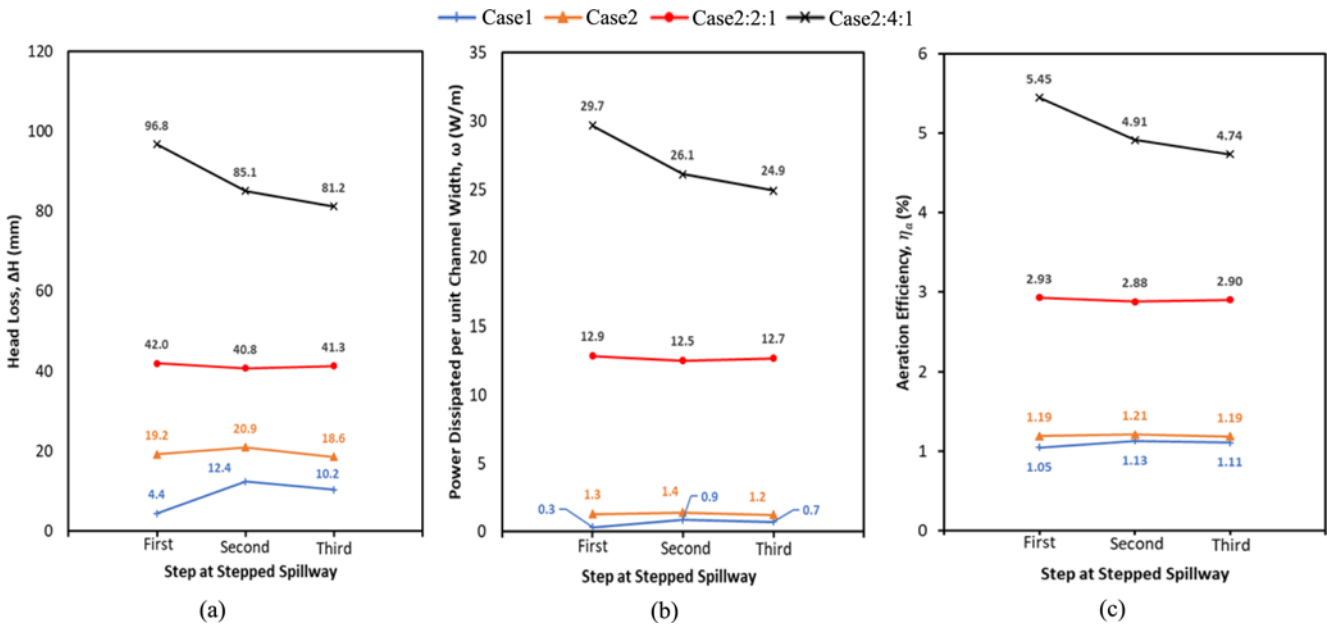


Fig. 22. The Plots of: (a) Head Loss, (b) Power Dissipated per Unit Channel Width, (c) Aeration Efficiency at Different Steps at Stepped Spillway Models in Case 1, Case 2 (Case 2: 2:1 and Case 2: 4:1)

of the water in the aeration and filtration systems.

Upon comparing the aeration performance between both stepped spillway models as given in Fig. 22, it is found that generally Case 2 generally possess higher values of power dissipated and aeration efficiency than Case 1. The increase in barrier height, 10 mm for Case 1 and 25 mm for Case 2, promotes the formation of hydraulic jump near the edge of step. This subsequently leads to the enhancement of energy dissipation of the flowing water, provided that the threshold value of barrier height is not exceeded. In spite of this finding, the aeration performance of Case 2 is still considered better as its aeration efficiency is higher than that of Case 1 for each step. This is evident by a higher average aeration efficiency of 1.20% in Case 2 as compared to 1.10% in Case 1.

The aeration efficiency of scale up for Case 2 by two times and four times bigger are also plotted in Fig. 22 whereby the aeration efficiency increases as the size of the model increase with average of 2.9% and 5.03%, respectively. Therefore, as the size of model increase the aeration of efficiency also increase. As discussed earlier, there will be more oxygen being dissolved since the aeration efficiency is now increase. As a result, the water quality of Case 2 configuration would be improved due to the substantial amount of dissolved oxygen content. In summary, it is proven that the dimension of configuration does affect the aeration performance of the cascade aerator system.

3.8 Oxygenation Content in the Aeration of Stepped Spillway

The amount of oxygen dissolved in the aerated water of the stepped spillway can be approximated based on the following mass balance formulation. By balancing the mass exchange between water and oxygen in air, the concentration of dissolved oxygen in water as a time function, $C(t)$ can be expressed as (Chanson, 1994; Gonzalez and Chanson, 2007):

$$\frac{dC}{dt} = k(C_{eq} - C) \quad (39)$$

$$C(t) = C_{eq} - (C_{eq} - C_0)e^{-kt} \quad (40)$$

where the equilibrium concentration of dissolving oxygen in water at 25°C is given by $C_{eq} = 8.3$ mg/L (Gheorghie et al., 2018); C_0 is the initial oxygen concentration in water and k is the mass transfer coefficient. The value of k for dissolution of oxygen into water can be determined by correlation fitting the experimental data into Eq. (2), and its value is approximately calculated as $8 \times 10^{-4} \text{ s}^{-1}$ (Huang et al., 2009). It should be noted that this value is only valid at ambient conditions with standard temperature of 10°C and atmospheric pressure P_{atm} ; while at 25°C and pressure, P , the mass transfer coefficient is modified as:

$$k' = 0.8775k \cdot \frac{P}{P_{atm}} \quad (41)$$

The concentration of dissolved oxygen in the water flow of the stepped spillway can be determined jointly based on Eqs. (30) and (31). The water in stepped spillway reservoir is assumed

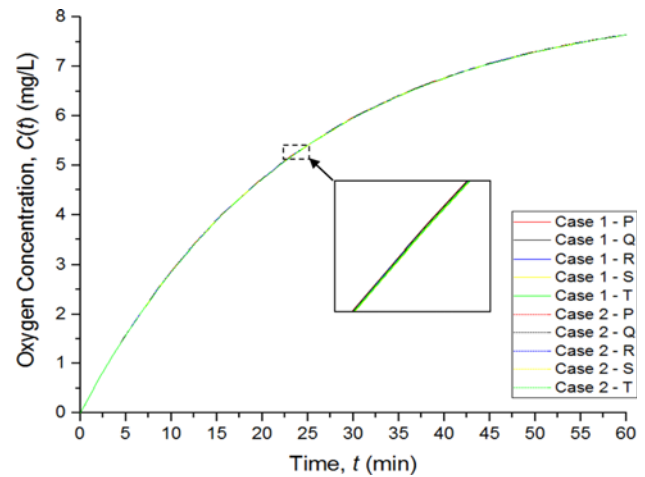


Fig. 23. Time Variations of Dissolved Oxygen Concentration in the Steady Continuous Water Flows at Five Selected Points (P , Q , R , S and T) along the Stepped Spillway Models in Case 1 and Case 2

to be perfectly pure without any dissolved particle or gas, i.e. $C_0 = 0$. Moreover, the temperature is regarded to remain constant throughout the flow along the stepped spillway. Thus, it is seen that the only variable of influence is the value of k' indicating the water stagnant pressure, p at that vicinity. By considering the continuous steady flow of water along the stepped spillway, the time variation of oxygen concentration inside the water at the vicinity of fixed points P , Q , R , S and T of two different stepped spillway, Case 1 and Case 2 are plotted in Fig. 23. It appears that the oxygen concentration increases exponentially with time and it took over 1 hour to reach the saturated concentration of oxygen at that particular ambient condition.

The stepped spillway models in both cases comprises of only four steps and it barely took over one second to reach the lowest step. Therefore, the time interval of one hour described in Fig. 23 is rather too long and may not serve as useful explanation to our current research subject. Given the huge gap in the scale, the current formulation will provide some insight on the total amount of time required and also the number of steps in aeration system to substantially dissolve huge amount of oxygen into the water, provided that no dissolved oxygen escapes to air thereafter. This is generally valid for actual size stepped spillway.

The scaling effect on the current scaled-down stepped spillway model can be studied based on the dimensional homogeneity, i.e., the invariant of Reynolds number. Let x be one-dimensional characteristic scale length of the stepped spillway model, we would expect a relationship of $\nu x = \text{const.}$, where ν is the average flow's velocity. Thus, the water's speed would increase when the model is scaled up, and the flow time is tremendously reduced. Upon realizing that the scaling effect is solely affects the flow's kinematics, the formulation in determine the dissolved oxygen concentration in Eqs. (29) – (31) are viable.

Accordingly, to match our stepped spillway models, the plot of oxygen concentration variations was reconstructed with rescaled

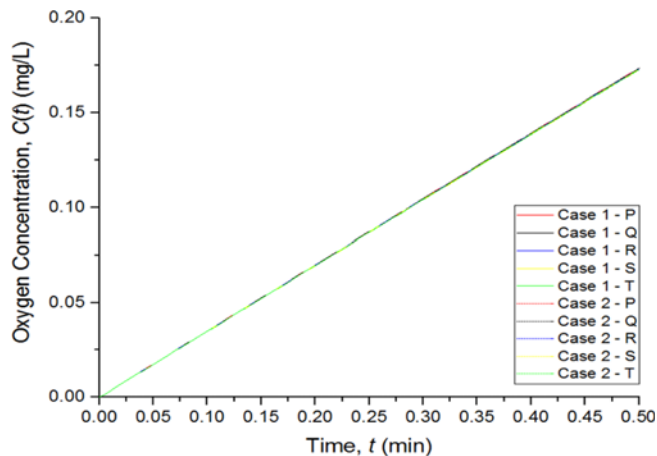


Fig. 24. Concentration of Oxygen in Water at Various Points in Both Configurations as a Function of Time, for a Short Range of Half Minutes (30 s)

time axis for a span of 30 seconds as illustrated in Fig. 24. Visual inspection reveals that the oxygen concentration in water increases directly proportionally with time as the flow progresses down the stepped spillways. It is also found that the variations were indistinguishable based on the spillway configurations and its positions as all graphs are extremely close to each other and collapsed into a straight line. It is assumed that the water flows at each point for both spillway models having constant temperature of 25°C and the gauge pressure at each those locations did not vary too much. Thus, the oxygen concentration in water can be thought to be invariant between both configurations, as described in Case 1 and Case 2.

As previously in Section 3.7, it was argued that there is an increase in average aeration efficiency from 1.10% in Case 1 to 1.20% in Case 2 due to double increase in barrier height of the stepped spillway from 10 mm to 25 mm, thus improving the aeration quality of the water by promoting more dissolution of oxygen. However, such finding may not able be visualized in the oxygen concentration plots in Figs. 23 and 24. This is due to constant water temperature and almost similar flow's pressure at all points across both models, as argued previously.

Alternatively, the aeration performance of both stepped spillway models can be studied in term of the input power drawn. The fundamental calculation of aeration efficiency is in fact based on the ratio of the amount of oxygen dissolved in water to the power drawn by the aeration system. While the oxygen concentration in the water is found to be approximately similar in both configurations, the higher aeration efficiency determined in Case 2 justified that its aeration system draws lesser power input. The high velocity flow in Case 2 as well as its higher barrier promotes the formation of turbulent regime and vortices which in turn aids in the formation of much more vigorous hydraulic jump that would dissipates more power from the incoming water flow during the aeration process. This will further produce more macro scale vortices that will enable more air entrainment and able to sustain the aeration process itself by

drawing more energy from the flow instead of the system. Finally, the power drawn from the reservoir to achieve necessary hydraulic jump would be reduced with prominent hydraulic jump effect can be achieved.

4. Conclusions

SPH based numerical study was performed on two near-identical stepped spillway configurations, Case 1 and Case 2, with different barrier heights of 10 mm and 25 mm, respectively. This paper presented the effect of varying the barrier height of the stepped spillway on the flow pattern in terms of the velocity, pressure as well as the filtration, aeration and oxygenation performances. Our SPH models are thoroughly validated using a promising experimental approach, known as PIV. Similar flow patterns are observed along the steps being attained using both SPH and PIV methods. Moreover, for the flow velocities obtained at different selected locations based on the numerical SPH spillway model are found to agree well with its corresponding PIV experimental data. Generally, both stepped configurations in Case 1 and Case 2 displayed identical flow pattern with nappe flow regime being developed. This can be viewed as the discharge of water in a succession of free-falling nappes from one step pool to the other. While the flow along stepped spillway is mainly classified as highly ordered laminar flow; however, water swirling, turbulence flow and vortices can be observed particularly at the second and third steps of model in Case 2. Overall, it is found that higher velocity and lower pressure flow are being observed in Case 2, thus effectively concluded the impact of increasing the height of the barrier based on it flow dynamic in the stepped spillway.

The aeration performance, the head loss and power dissipated of the water jet during the occurrence of hydraulic jump are shown to be higher in Case 2. Consequently, the average aeration efficiency improved from 1.10% in Case 1 to 1.20% in Case 2 by increasing the barrier's height. In the meantime, all the head loss, power dissipated and aeration efficiency for both cases increase as the flow ascends down the step with the highest values being registered at the third step. Furthermore, the aeration efficiency also increases from the scale up Case 2 with two and four times bigger with average of 2.9% and 5.03%, respectively. The dissolved oxygen concentration in the water flow is studied theoretically and is found to be solely dependent on the flow pressure. Nevertheless, due to fairly similar gauge pressure of flow at all locations in both models, the oxygen dissolution variation can be assumed to be identical for both configurations.

The higher aeration efficiency in Case 2 suggested that higher barrier would promote the occurrence of more vigorous hydraulic jump that will cause strong turbulent mixing that is associated with significant air entrainment. This will substantially decrease the power drawn from the reservoir for this aeration process, as more power will be dissipated by the flow itself. Therefore, the transfer of oxygen into the water is concluded to be more effective. Overall, the dimension of the stepped spillway particularly

the barrier is found to be crucial on the flow behavior as well as the aeration and oxygenation performances. In the near future, this method can be applied on real scale by using high performance computer (HPC).

Acknowledgements


The work was supported by the Fundamental Research Grant Scheme (FRGS) (Grant number: FRGS/1/2019/TK03/USM/03/1), Research University (RU) (Grant number: 8014071), FRGS under Ministry of Higher Education of Malaysia (Grant number: 7611800357) and TNB Seeding Fund PD: U-TG-RD-18-05.

ORCID

Aqil Azman  <https://orcid.org/0000-0001-5073-4801>

Fei Chong Ng  <https://orcid.org/0000-0002-7045-4599>

Aizat Abas  <https://orcid.org/0000-0002-7014-0370>

Mohd. Remy Rozainy M. A. Z.  <https://orcid.org/0000-0002-4959-6584>

References

- Albano R, Sole A, Mirauda D, Adamowski J (2016) Modelling large floating bodies in urban area flash-floods via a Smoothed Particle Hydrodynamics model. *Journal of Hydrology* 541(Part A):344-358, DOI: 10.1016/j.jhydrol.2016.02.009
- Amador A, Van der Graaf G, Juny M, Dolz J, Sanchez-Tembleque F, Agudo J (2004) Characterization of the flow field in a stepped spillway by PIV. Proceedings of 12th symposium: Applications laser to fluid mechanics, July 12-15, Lisbon, Portugal
- ANSYS Inc. (2006) FLUENT 6.3 user's guide. Chapter 10: Modeling turbulence. Fluent Inc., Lebanon, PA, USA
- António A, Martí S-J, Josep D (2009) Developing flow region and pressure fluctuations on steeply sloping stepped spillways. *Journal of Hydraulic Engineering* 135(12):1092-1100, DOI: 10.1061/(ASCE)HY.1943-7900.0000118
- Aras E, Berkun M (2010) Comparison of stepped and smooth spillway effects on stream reaeration. *Water SA* 36(3):309-314
- Chang T-J, Kao H-M, Chang K-H, Hsu M-H (2011) Numerical simulation of shallow-water dam break flows in open channels using smoothed particle hydrodynamics. *Journal of Hydrology* 408(1-2):78-90, DOI: 10.1016/j.jhydrol.2011.07.023
- Chanson H (1994) Hydraulics of nappe flow regime above stepped chutes and spillways. *Australian Civil/Structural Engineering Transactions* 36(1):69-76
- Chanson H, Toombes L (2002) Air-water flows down stepped chutes: Turbulence and flow structure observations. *International Journal of Multiphase Flow* 28(11):1737-1761, DOI: 10.1016/S0301-9322(02)00089-7
- Chatila JG, Jurdi BR (2004) Stepped spillway as an energy dissipater. *Canadian Water Resources Journal* 29(3):147-158, DOI: 10.4296/cwrj147
- Chen Q, Dai G-Q, Liu H-W (2002) Numerical simulation for the stepped spillway overflow with turbulence model. *Journal of Hydrodynamics* 14(2):58-63
- Colagrossi A, Landrini M (2003) Numerical simulation of interfacial flows by smoothed particle hydrodynamics. *Journal of Computational Physics* 191(2):448-475, DOI: 10.1016/S0021-9991(03)00324-3
- Crespo A (2008) Application of the Smoothed Particle Hydrodynamics model SPPhysics to free-surface hydrodynamics. PhD Thesis, University of Vigo, Pontevedra, Spain
- Dalrymple R, Knio O (2001) SPH modeling of water waves. Fourth conference on coastal dynamics, June 11-15, Lund, Sweden, 779-787
- de Carvalho R, Táboas Amador A, Zhang C, Tang H (2009) Physical and numerical investigation of the skimming flow over a stepped spillway BT - Advances in water resources and hydraulic engineering. Springer, Berlin, Germany, 1767-1772
- Dilts G (1999) Moving-least-squares-particle hydrodynamics — I. Consistency and stability. *International Journal for Numerical Methods in Engineering* 44(8):1115-1155, DOI: 10.1002/(SICI)1097-0207(19990320)44:8<1115::AID-NME547>3.0.CO;2-L
- Felder S, Chanson H (2011) Energy dissipation down a stepped spillway with non-uniform step heights. *Journal of Hydraulic Engineering* 137(11):1543-1548, DOI: 10.1061/(ASCE)HY.1943-7900.0000455
- Felder S, Chanson H (2013) Aeration, flow instabilities, and residual energy on pooled stepped spillways of embankment dams. *Journal of Irrigation and Drainage Engineering* 139(10):880-887, DOI: 10.1061/(ASCE)IR.1943-4774.0000627
- Ferrari A (2010) SPH simulation of free surface flow over a sharp-crested weir. *Advances in Water Resources* 33(3):270-276, DOI: 10.1016/j.advwatres.2009.12.005
- Gheorghe G, Dontu O, Băran N, Corina Moga I, Mihaela C, Tămă-anu E (2018) Researches on the measurement of the dissolved oxygen concentration in stationary waters. Proceedings of the international conference of mechatronics and cyber-mixmechatronics, September 6-7, Bucharest, Romania, 29-40
- Gingold RA, Monaghan JJ (1977) Smoothed particle hydrodynamics: Theory and application to non-spherical stars. *Monthly Notices of the Royal Astronomical Society* 181(3):375-389, DOI: 10.1093/mnras/181.3.375
- Gonzalez C, Chanson H (2007) Hydraulic design of stepped spillways and downstream energy dissipators for embankment dams. *Dam Engineering* 17(4):223-244
- Guenther P, Felder S, Chanson H (2013) Flat and pooled stepped spillways for overflow weirs and embankments: Cavity flow processes, flow aeration and energy dissipation. International Workshop on Hydraulic Design of Low-Head Structures, Aachen, Germany, 77-86
- Hamedí A, Malekmohammadi I, Mansoori A, Roshanaei H (2012) Energy dissipation in stepped spillway equipped with inclined steps together with end sill. Proceedings of 4th international conference on computational intelligence and communication networks, November 3-5, Mathura, India, 638-642, DOI: 10.1109/CICN.2012.109
- Huang W, Wu C, Xia W (2009) Oxygen transfer in high-speed surface aeration tank for wastewater treatment: Full-scale test and numerical modeling. *Journal of Environmental Engineering* 135(8):684-691, DOI: 10.1061/(ASCE)EE.1943-7870.0000023
- Husain S (2016) Open boundary condition for a numerical sph method to characterize the flow in open channels. *ZANCO Journal of Pure and Applied Sciences* 28(2):207-2016, DOI: 10.21271/zjpas.v28i2.821
- Husain SM, Muhammed JR, Karunarathna HU, Reeve DE (2014) Investigation of pressure variations over stepped spillways using smooth particle hydrodynamics. *Advances in Water Resources* 66:52-69, DOI: 10.1016/J.ADVWATRES.2013.11.013
- Jonsson P, Jónsén P, Andreasson P, Lundström T, Hellström JG (2015) Modelling dam break evolution over a wet bed with smoothed

- particle hydrodynamics: A parameter study. *Engineering* 7:248-260, DOI: [10.4236/eng.2015.75022](https://doi.org/10.4236/eng.2015.75022)
- Kao H-M, Chang T-J (2012) Numerical modeling of dam-break-induced flood and inundation using smoothed particle hydrodynamics. *Journal of Hydrology* 448-449:232-244, DOI: [10.1016/j.jhydrol.2012.05.004](https://doi.org/10.1016/j.jhydrol.2012.05.004)
- Kokila K, Divya R (2015) Analysis and design of cascade aerator construction for mettur water treatment plant. National Conference on Research Advances in Communication, Computation, Electrical Science and Structures (NCRACCESS-2015), Seventh Sense Research Group, Tiruchirappalli, India, 42-46
- Kucukali S, Cokgor S (2009) Energy concept for predicting hydraulic jump aeration efficiency. *Journal of Environmental Engineering* 13(2):105-107, DOI: [10.1061/\(ASCE\)0733-9372\(2009\)135:2\(105\)](https://doi.org/10.1061/(ASCE)0733-9372(2009)135:2(105))
- Kumcu SY (2017) Investigation of flow over spillway modeling and comparison between experimental data and CFD analysis. *KSCE Journal of Civil Engineering* 21(6):994-1003, DOI: [10.1007/s12205-016-1257-z](https://doi.org/10.1007/s12205-016-1257-z)
- Lawler D (1993) The measurement of river bank erosion and lateral channel change: A review. *Earth Surface Processes and Landforms* 18(9):777-821, DOI: [10.1002/esp.3290180905](https://doi.org/10.1002/esp.3290180905)
- Monaghan JJ (1989) On the problem of penetration in particle methods. *Journal of Computational Physics* 82(1):1-5, DOI: [10.1016/0021-9991\(89\)90032-6](https://doi.org/10.1016/0021-9991(89)90032-6)
- Monaghan JJ (1992) Smoothed particle hydrodynamics. *Annual Review of Astronomy and Astrophysics* 30:543-574, DOI: [10.1146/annurev.aa.30.090192.002551](https://doi.org/10.1146/annurev.aa.30.090192.002551)
- Mostefa G, Kheira B, Djehiche A, Naima D (2015) Study of the effect of the rate flow and the slope of the channel on the energy dissipation in the stepped channels: Proposing an empirical models. *Procedia Engineering* 118:1044-1051, DOI: [10.1016/j.proeng.2015.08.547](https://doi.org/10.1016/j.proeng.2015.08.547)
- Panizzo A (2004) Physical and numerical modelling of subaerial landslide generated waves. PhD Thesis, Università degli Studi dell'Aquila, L'Aquila, Italy
- Peltier Y, Dewals B, Archambeau P, Piroton M, Erpicum S (2017) Pressure and velocity on an ogee spillway crest operating at high head ratio: Experimental measurements and validation. *Journal of Hydro-environment Research* 19:128-136, DOI: [10.1016/j.jher.2017.03.002](https://doi.org/10.1016/j.jher.2017.03.002)
- Rathinakumar V, Dhinakaran G, Cr S (2014) Assessment of aeration capacity of stepped cascade system for selected geometry. *International Journal of ChemTech Research* 6(1):254-262
- Rebollo JJ, Blas M de, López D, Diaz R, Marivela R (2010) Hydrodynamic verification with SPH of under gate flow in the Alarcón spillway (Spain). First European IAHR Congress, Edinburgh, UK
- Roushangar K, Akhgar S, Salmasi F, Shiri J (2014) Modeling energy dissipation over stepped spillways using machine learning approaches. *Journal of Hydrology* 508:254-265, DOI: [10.1016/j.jhydrol.2013.10.053](https://doi.org/10.1016/j.jhydrol.2013.10.053)
- Saunders K, Prakash M, Cleary P, Cordell M (2014) Application of Smoothed Particle Hydrodynamics for modelling gated spillway flows. *Applied Mathematical Modelling* 38(17-18):4308-4322, DOI: [10.1016/j.apm.2014.05.008](https://doi.org/10.1016/j.apm.2014.05.008)
- Shahheydari H, Nodoshan EJ, Barati R, Moghadam MA (2015) Discharge coefficient and energy dissipation over stepped spillway under skimming flow regime. *KSCE Journal of Civil Engineering* 19(4):1174-1182, DOI: [10.1007/s12205-013-0749-3](https://doi.org/10.1007/s12205-013-0749-3)
- Stefan F, Hubert C (2014) Effects of step pool porosity upon flow aeration and energy dissipation on pooled stepped spillways. *Journal of Hydraulic Engineering* 140(4):4014002, DOI: [10.1061/\(ASCE\)HY.1943-7900.0000858](https://doi.org/10.1061/(ASCE)HY.1943-7900.0000858)
- Tabbara M, Chatila J, Awwad R (2005) Computational simulation of flow over stepped spillways. *Computers & Structures* 83(27):2215-2224, DOI: [10.1016/j.compstruc.2005.04.005](https://doi.org/10.1016/j.compstruc.2005.04.005)
- Thakare SW, Tatewar SP (2009) Discussion of "Inception point and air concentration in flows on stepped chutes lined with wedge-shaped concrete blocks" by António T. Relvas and António N. Pinheiro. *Journal of Hydraulic Engineering* 136(1):28-30
- Toosi SLR, Ayyoubzadeh SA, Valizadeh A (2015) The influence of time scale in free surface flow simulation using smoothed particle hydrodynamics (SPH). *KSCE Journal of Civil Engineering* 19(9):765-770, DOI: [10.1007/s12205-012-0477-0](https://doi.org/10.1007/s12205-012-0477-0)
- Twort AC, Ratnayaka DD, Brandt MJBT-WS (2000) 10 - Hydraulics, 5th edition. Butterworth-Heinemann, London, UK, 463-498
- Vosoughifar HR, Dolatshah A, Kazem Sadat Shokouhi S, Reza Hashemi Nezhad S (2013) Evaluation of fluid flow over stepped spillways using the finite volume method as a novel approach. *Strojnikski Vestnik - Journal of Mechanical Engineering* 59(5):301-310, DOI: [10.5545/sv-jme.2012.669](https://doi.org/10.5545/sv-jme.2012.669)
- Wang S, Hou D, Wang C (2012) Aerator of stepped chute in murum hydropower station. *Procedia Engineering* 28:803-807, DOI: [10.1016/j.proeng.2012.01.813](https://doi.org/10.1016/j.proeng.2012.01.813)
- Wu J, Zhang B, Ma F (2013) Inception point of air entrainment over stepped spillways. *Journal of Hydrodynamics* 25(1):91-96, DOI: [10.1016/S1001-6058\(13\)60342-X](https://doi.org/10.1016/S1001-6058(13)60342-X)
- Xu X (2016) An improved SPH approach for simulating 3D dam-break flows with breaking waves. *Computer Methods in Applied Mechanics and Engineering* 311:723-742, DOI: [10.1016/j.cma.2016.09.002](https://doi.org/10.1016/j.cma.2016.09.002)
- Xu X, Ouyang J, Yang B, Liu Z (2013) SPH simulations of three-dimensional non-Newtonian free surface flows. *Computer Methods in Applied Mechanics and Engineering* 256:101-116, DOI: [10.1016/j.cma.2012.12.017](https://doi.org/10.1016/j.cma.2012.12.017)
- Zhang A, Sun P, Ming F (2015) An SPH modeling of bubble rising and coalescing in three dimensions. *Computer Methods in Applied Mechanics and Engineering* 294:189-209, DOI: [10.1016/j.cma.2015.05.014](https://doi.org/10.1016/j.cma.2015.05.014)